Published November 14, 2011

the LSK phenotype (Fig. 3 F), indicating that loss of GFP correlates with phenotypic differentiation. To confirm the differential phenotype of the GFP$^-$ and GFP$^+$ cells after culture reflected their functional status, we compared their ability to form colonies in methylcellulose. GFP$^+$ cells yielded significantly more colonies than GFP$^-$ cells (Fig. 3 G), suggesting that functionally primitive HSCs predominantly reside in the GFP$^+$ fraction. Collectively, these data indicate that in vitro culture of LSK GFP$^+$ cells leads to generation of GFP$^-$ cells that are more differentiated, and lend credence to the use of GFP as a fluorescent sensor for the differentiation state of hematopoietic cells.

To determine the cell-cycle distribution of LSK GFP$^-$ and LSK GFP$^+$ cells, we performed Hoechst 33342 and pyronin Y staining, which revealed that the majority of LSK GFP$^+$ cells were in G_0 phase, whereas a significant proportion of LSK GFP$^-$ cells were actively cycling (Fig. 3 H). These data indicate that, within HSPCs, Evi1 expression represents a functionally distinct population that remains in an undifferentiated and quiescent state.

Evi1 expression marks in vivo long-term multilineage repopulating HSCs in adult BM

Based on the aforementioned data, we hypothesized that Evi1 expression would have the potential to effectively mark long-term multilineage repopulating HSCs. To examine this issue, we performed a CRA, in which 500 purified LSK GFP$^-$ or LSK GFP$^+$ cells were transplanted with 2×10^5 competitor BM cells into lethally irradiated recipients (Fig. S1 A). At 16 wk after transplantation, flow cytometric analysis of donor-derived cells revealed long-term reconstitution in all recipients transplanted with LSK GFP$^+$ cells (Fig. 4 A). Moreover, LSK GFP$^+$ cells displayed multilineage potential with robust contribution to myeloid, B, and T cells in peripheral blood (PB) as well as the LSK

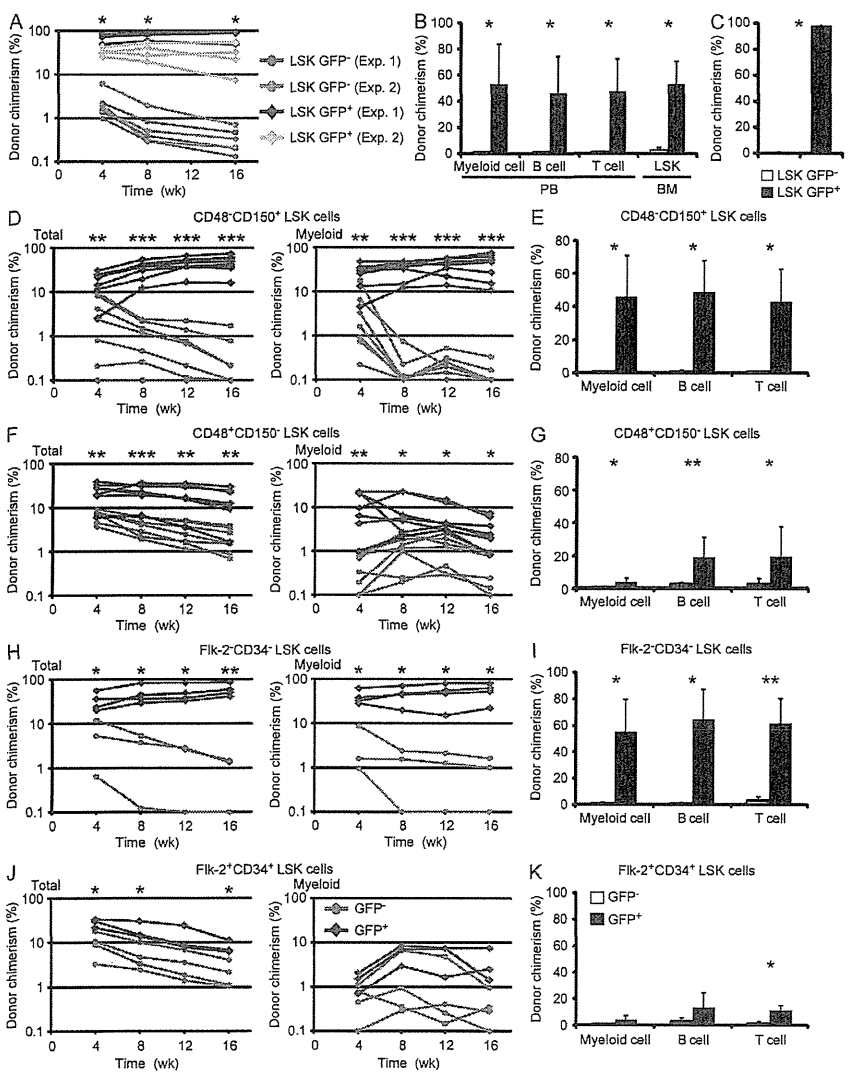

Figure 4. Evi1 expression marks in vivo long-term multilineage repopulating HSCs in adult BM. (A and B) PB donor chimerism in CRAs, in which 500 LSK GFP$^-$ or LSK GFP$^+$ cells sorted from *Evi1*$^{+/GFP}$ mice (Ly5.2) were transplanted into lethally irradiated recipients (Ly5.1) together with 2×10^5 competitor BM cells (Ly5.1 × Ly5.2). (A) Percentages of donor-derived cells (Ly5.2) in PB after transplantation are shown. Each dot indicates an individual recipient mouse (*, $P < 0.005$; $n = 6$–7 from 2 independent experiments). (B) Percentages of donor-derived cells (Ly5.2) in myeloid, B, and T cells of PB and LSK cells of BM 16 wk after transplantation. Recipient mice in experiment 1 were used for the analysis of BM (*, $P < 0.01$; $n = 6$–7 for PB and $n = 3$ for BM). (C) Percentages of donor-derived cells (Ly5.2) in PB of secondary recipient mice (Ly5.1) 16 wk after transplantation. Recipient mice in experiment 1 were used for secondary transplantation (*, $P < 0.0001$, $n = 3$). (D–K) PB donor chimerism in CRAs, in which 100 CD48$^-$ CD150$^+$ LSK GFP$^-$ or CD48$^-$ CD150$^+$ LSK GFP$^+$ cells (D and E; $n = 7$–8), or 500 CD48$^+$ CD150$^-$ LSK GFP$^-$ or CD48$^+$ CD150$^-$ LSK GFP$^+$ cells (F and G; $n = 7$), or 100 Flk-2$^-$ CD34$^-$ LSK GFP$^-$ or Flk-2$^-$ CD34$^-$ LSK GFP$^+$ cells (H and I; $n = 3$–4), or 500 Flk-2$^+$ CD34$^+$ LSK GFP$^-$ or Flk-2$^+$ CD34$^+$ LSK GFP$^+$ cells (J and K; $n = 3$–4) sorted from *Evi1*$^{+/GFP}$ mice (Ly5.1) were transplanted into lethally irradiated recipients (Ly5.2) together with 2×10^5 competitor BM cells (Ly5.2). (D, F, H, and J) Percentages of donor-derived cells (Ly5.1) in total (left) and myeloid cells (right) of PB after transplantation are shown. Each dot indicates an individual recipient mouse (*, $P < 0.05$; **, $P < 0.005$; ***, $P < 0.0005$). (E, G, I, and K) Percentages of donor-derived cells (Ly5.1) in myeloid, B, and T cells of PB 16 wk after transplantation (*, $P < 0.05$; **, $P < 0.005$). Data represent mean ± SD.

Published November 14, 2011

JEM

fraction in BM (Fig. 4 B). In contrast, LSK GFP$^-$ cells yielded an almost total inability to generate long-term chimerism (Fig. 4, A and B), which suggests that this population is devoid of self-renewal activity. To confirm the in vivo repopulating capacity of LSK GFP$^+$ cells, we performed secondary transplantation. Similarly, LSK GFP$^+$ cells showed remarkable long-term reconstitution, whereas LSK GFP$^-$ cells consistently failed to produce detectable donor-derived cells (Fig. 4 C), demonstrating that in vivo long-term multilineage repopulating cells are exclusively enriched in the LSK GFP$^+$ fraction in adult BM.

To further refine our analysis designating Evi1 expression as a robust and reliable HSC marker, we compared the repopulating capacity of GFP$^-$ and GFP$^+$ cells within the CD48$^-$ CD150$^+$ LSK fraction, which is enriched for LT-HSCs (Fig. S1 B). Intriguingly, CD48$^-$ CD150$^+$ LSK GFP$^+$ cells exhibited long-term multilineage reconstitution, whereas no engraftment was observed in recipients of CD48$^-$ CD150$^+$ LSK GFP$^-$ cells (Fig. 4, D and E), suggesting that long-term repopulating HSCs predominantly reside in the GFP$^+$ fraction even within the highly subfractionated LT-HSC fraction. We then examined whether Evi1 expression is associated with repopulating capacity in the CD48$^+$ CD150$^-$ LSK fraction, which is enriched for ST-HSCs/MPPs with limited self-renewal activity (Fig. S1 B). Although CD48$^+$ CD150$^-$ LSK GFP$^-$ cells provided only a transient reconstitution, CD48$^+$ CD150$^-$ LSK GFP$^+$ cells showed declining, but sustained engraftment 16 wk after transplantation (Fig. 4 F). In contrast to CD48$^-$ CD150$^+$ LSK GFP$^+$ cells, CD48$^+$ CD150$^-$ LSK GFP$^+$ cells mediated faint myeloid but superior lymphoid reconstitution (Fig. 4, F and G). Although it is controversial whether CD48$^+$ CD150$^-$ LSK cells are transiently reconstituting MPPs/ST-HSCs or lymphoid-biased LT-HSCs with limited long-term engraftment and strong predominance of lymphoid reconstitution (Kiel et al., 2005; Weksberg et al., 2008; Grassinger et al., 2010), Evi1-expressing cells possess higher repopulating capacity within this fraction. When we subfractionated the LSK fraction according to CD34 and Flk-2 expression, and compared the repopulating capacity of GFP$^-$ and GFP$^+$ cells within these subsets (Fig. S1 C), we obtained similar results to the aforementioned findings using SLAM markers (Fig. 4, H–K). These data reveal that, irrespective of the combination of HSC surface markers used, GFP$^+$ cells are the exclusive reservoir of HSC activity, with no reconstitution ability being observed in GFP$^-$ cells within the LT-HSC compartment. Altogether, our results demonstrate that Evi1 expression can further augment the conventional HSC purification strategy, and suggest that Evi1-IRES-GFP knock-in mice allow us to functionally identify HSCs on the ground of self-renewal capacity.

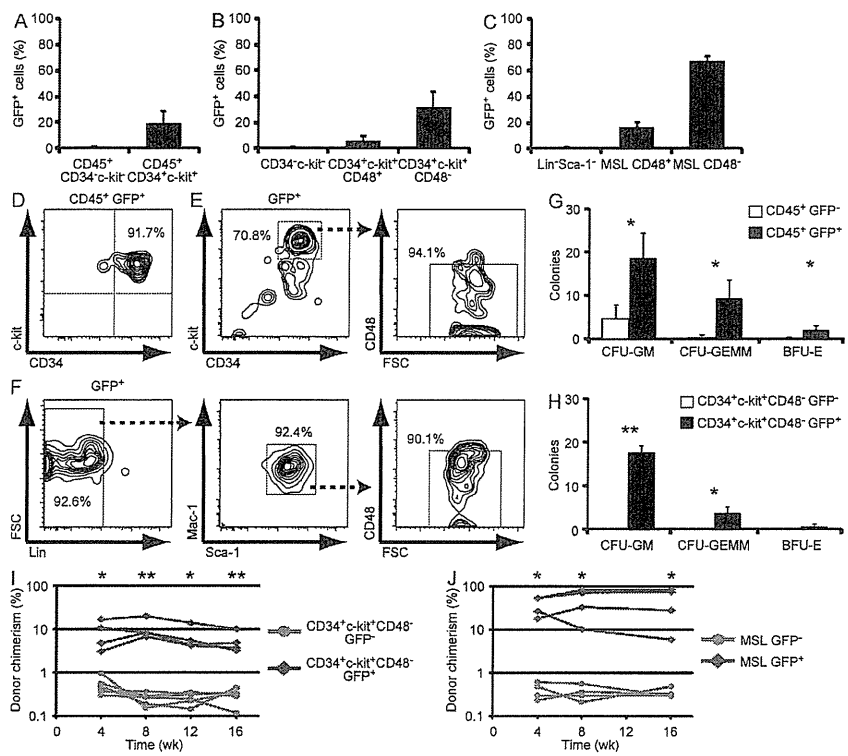

Figure 5. Evi1 expression marks in vivo long-term multilineage repopulating HSCs in embryo. (A–C) Frequency of GFP$^+$ cells in each subpopulation of E10.5 AGM (A; $n = 5$) or E12.5 placenta (B; $n = 3$) or E14.5 FL (C; $n = 5$) from *Evi1*$^{+/GFP}$ embryos. (D–F) FACS analysis of expression of CD34 and c-kit on CD45$^+$ GFP$^+$ cells from E10.5 AGM (D) or CD34, c-kit, and CD48 on GFP$^+$ cells from E12.5 placenta (E) or Lin, Mac-1, Sca-1, and CD48 on GFP$^+$ cells from E14.5 FL (F) in *Evi1*$^{+/GFP}$ embryos. Data are representative of 2 to 10 independent experiments. (G and H) Numbers of CFU-GM, CFU-GEMM, and BFU-E colonies derived from 100 CD45$^+$ GFP$^-$ and CD45$^+$ GFP$^+$ cells sorted from E10.5 AGM (G; $n = 3$), or 100 CD34$^+$ c-kit$^+$ CD48$^-$ GFP$^-$ and CD34$^+$ c-kit$^+$ CD48$^-$ GFP$^+$ cells sorted from E12.5 placenta (H; $n = 3$) in *Evi1*$^{+/GFP}$ embryos (*, $P < 0.05$; **, $P < 0.0005$). (I) PB donor chimerism in CRAs, in which 500 CD34$^+$ c-kit$^+$ CD48$^-$ GFP$^-$ or CD34$^+$ c-kit$^+$ CD48$^-$ GFP$^+$ cells sorted from E12.5 placenta of *Evi1*$^{+/GFP}$ embryos (Ly5.1 × Ly5.2) were transplanted into lethally irradiated recipients (Ly5.2) together with 2×10^5 competitor BM cells (Ly5.2). Percentages of donor-derived cells (Ly5.1 × Ly5.2) in PB after transplantation are shown. Each dot indicates an individual recipient mouse (*, $P < 0.05$; **, $P < 0.005$; $n = 4$–6). (J) PB donor chimerism in CRAs, in which 500 MSL GFP$^-$ or MSL GFP$^+$ cells sorted from E14.5 FL of *Evi1*$^{+/GFP}$ embryos (Ly5.2) were transplanted into lethally irradiated recipients (Ly5.1 × Ly5.2) together with 2×10^5 competitor BM cells (Ly5.1 × Ly5.2). Percentages of donor-derived cells (Ly5.2) in PB weeks after transplantation are shown. Each dot indicates an individual recipient mouse (*, $P < 0.05$; $n = 4$). Data represent mean ± SD.

Published November 14, 2011

Evi1 expression marks in vivo long-term multilineage repopulating HSCs in embryo

The formation of blood cells begins in the yolk sac of the embryo, and then shifts to the aorta-gonad-mesonephros (AGM) region, and then sequentially to the placenta, fetal liver (FL), and adult BM. There are several major phenotypic and functional differences between fetal and adult HSCs in surface marker profile, cell cycle status, self-renewal potential, gene expression profile, and regulatory mechanism (Mikkola and Orkin, 2006; Orkin and Zon, 2008). Fetal HSCs, in particular, divide rapidly and undergo massive expansion, whereas adult HSCs are mostly quiescent (Bowie et al., 2006). It is known that Evi1 is highly expressed in the yolk sac, paraaortic splanchnopleura, and HSPCs ($CD45^+$ $CD34^+$ c-kit^+) in early embryo (Yuasa et al., 2005). Therefore, we sought to determine whether Evi1 expression can mark fetal HSCs despite their distinct features from adult HSCs, and thus analyzed the expression pattern of GFP in $Evi1^{+/GFP}$ embryos. As expected, GFP expression was highly restricted to HSPCs in the embryonic tissues; $CD45^+$ $CD34^+$ c-kit^+ cells in embryonic day 10.5 (E10.5) AGM, $CD34^+$ c-kit^+ $CD48^-$ cells in E12.5 placenta, and Mac-1^+ Sca-1^+ Lin^- (MSL) $CD48^-$ cells in E14.5 FL (Fig. 5, A–C; Takakura et al., 2000; Kim et al., 2006; McKinney-Freeman et al., 2009). When the distribution of GFP^+ cells in the fetal hematopoietic system was analyzed, most GFP^+ cells exhibited the HSPC-specific marker profile in all embryonic tissues examined (Fig. 5, D–F), indicating the predominant expression of Evi1 in HSPCs during fetal hematopoiesis.

To determine whether Evi1 expression is associated with hematopoietic activity in the embryonic tissues, we performed colony-forming assays in vitro using $CD45^+$ GFP^- and $CD45^+$ GFP^+ cells from E10.5 AGM, and found that $CD45^+$ GFP^+ cells contained almost all colony-forming cells, with few detectable hematopoietic colonies in $CD45^+$ GFP^- cells (Fig. 5 G). In the same manner, within the $CD34^+$ c-kit^+ $CD48^-$ fraction from E12.5 placenta of $Evi1^{+/GFP}$ embryos, colony-forming activity was exclusively present in GFP^+ cells, regardless of colony type (Fig. 5 H). These data suggest that clonogenic hematopoietic progenitors predominantly reside in the Evi1-expressing fraction in fetal hematopoiesis.

To examine whether Evi1 expression would have the potential to effectively mark long-term repopulating HSCs in embryo, we performed a CRA using sorted $CD34^+$ c-kit^+ $CD48^-$ GFP^- and $CD34^+$ c-kit^+ $CD48^-$ GFP^+ cells from E12.5 placenta of $Evi1^{+/GFP}$ embryos (Fig. S2 A). It was obvious that $CD34^+$ c-kit^+ $CD48^-$ GFP^+ cells contributed to the long-term reconstitution of irradiated recipients, whereas donor chimerism was almost undetectable in mice transplanted with $CD34^+$ c-kit^+ $CD48^-$ GFP^- cells (Fig. 5 I), which is in agreement with the results obtained with their adult counterparts. To further assess whether Evi1 expression can enrich long-term repopulating HSCs in embryo, we performed a CRA using purified MSL GFP^- and MSL GFP^+ cells from E14.5 FL (Fig. S2 B). Along with cells in E12.5 placenta, MSL GFP^+ cells gave rise to long-term multilineage reconstitution, whereas no engraftment was observed in recipients of MSL GFP^- cells (Fig. 5 J). These results indicate that fetal HSCs with active *Evi1* transcription exclusively harbor stem cell activity. Collectively, despite the functional differences between fetal and adult HSCs, Evi1 expression marks long-term multilineage repopulating HSCs throughout ontogeny, suggesting a specific relationship between Evi1 expression and HSC self-renewal capacity.

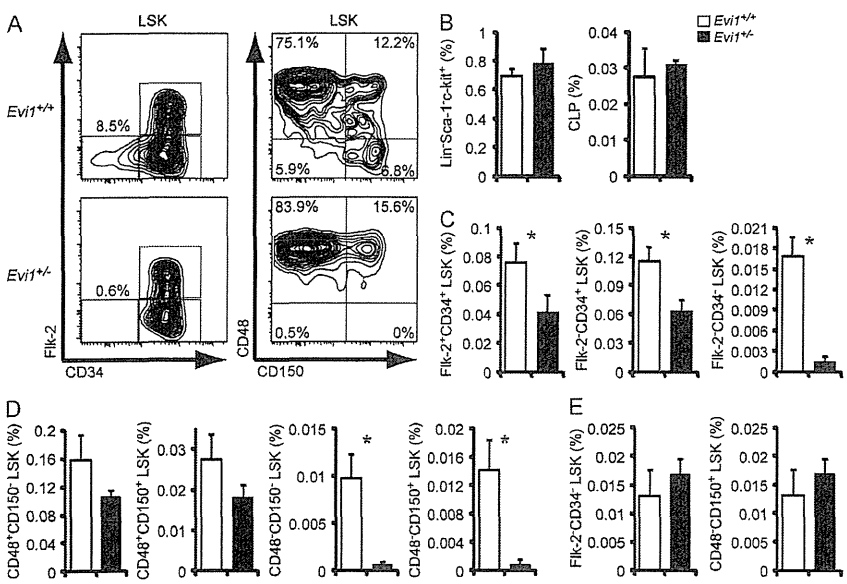

Figure 6. Evi1 heterozygosity leads to an almost complete loss of LT-HSCs in a cell-autonomous manner. (A) FACS analysis of expression of Flk-2 and CD34 or CD48 and CD150 on LSK cells in BM from $Evi1^{+/+}$ and $Evi1^{+/-}$ mice. Data are representative of at least three independent experiments. (B) Frequency of myeloid (Lin^- $Sca\text{-}1^-$ c-kit^+) and lymphoid progenitors (CLPs) in BM from $Evi1^{+/+}$ and $Evi1^{+/-}$ mice ($n = 3$). (C) Frequency of Flk-2^+ $CD34^+$, Flk-2^- $CD34^+$, and Flk-2^- $CD34^-$ subsets within LSK cells in BM from $Evi1^{+/+}$ and $Evi1^{+/-}$ mice (*, $P < 0.0001$; $n = 8$). (D) Frequency of $CD48^+$ $CD150^-$, $CD48^+$ $CD150^+$, $CD48^-$ $CD150^-$, and $CD48^-$ $CD150^+$ subsets within LSK cells in BM from $Evi1^{+/+}$ and $Evi1^{+/-}$ mice (*, $P < 0.01$; $n = 3$). (E) Reciprocal transplantation assay was performed by transplantation of 2×10^5 WT BM cells (Ly5.1) into lethally irradiated $Evi1^{+/+}$ or $Evi1^{+/-}$ mice (Ly5.2). Frequency of Flk-2^- $CD34^-$ LSK or $CD48^-$ $CD150^+$ LSK cells in BM of recipients 16 wk after transplantation is shown ($n = 4$). Data represent mean ± SD.

Published November 14, 2011

JEM

Evi1 heterozygosity leads to an almost complete loss of LT-HSCs in a cell-autonomous manner

The aforementioned observations led us to predict that Evi1 plays a functional role specifically in LT-HSCs. To clarify this issue, we analyzed heterozygous *Evi1* KO mice (*Evi1*$^{+/-}$). We previously showed that heterozygosity of Evi1 leads to decreased numbers of LSK and CD34$^-$ LSK cells, as well as impaired long-term repopulating activity (Goyama et al., 2008). In the current study, although Flk-2$^+$ CD34$^+$ and Flk-2$^-$ CD34$^+$ LSK cells were moderately decreased, Flk-2$^-$ CD34$^-$ LSK cells from *Evi1*$^{+/-}$ mice exhibited a marked reduction in frequency compared with WT controls (Fig. 6, A and C). Likewise, when LSK cells were subdivided according to SLAM markers, we observed substantial decreases in CD48$^-$ CD150$^-$ and CD48$^-$ CD150$^+$ LSK subsets (Fig. 6, A and D). Therefore, the number of each subpopulation within the LSK fraction in *Evi1*$^{+/-}$ mice was declined in proportion to their expression level of Evi1, indicating that Evi1 has a dominating effect on the maintenance of LT-HSCs. In contrast, there were no significant differences in BM cellularity and the frequencies of lymphoid and myeloid progenitors, and mature blood cells between *Evi1*$^{+/+}$ and *Evi1*$^{+/-}$ mice (Fig. 6 B and not depicted), indicating that the differentiation potential to all mature lineages and committed progenitors is normal in *Evi1*$^{+/-}$ mice. Collectively, these observations suggest that Evi1 serves as a specific regulator in the earliest stage of adult hematopoietic development.

To exclude the possibility that a defect of BM microenvironment could be responsible for the observed hematopoietic abnormalities in *Evi1*$^{+/-}$ mice, we performed reciprocal transplantation experiments, in which WT BM cells were transplanted into lethally irradiated *Evi1*$^{+/+}$ or *Evi1*$^{+/-}$ mice. At 16 wk after transplantation, flow cytometric analysis showed no differences in the percentages of Flk-2$^-$ CD34$^-$ LSK or CD48$^-$ CD150$^+$ LSK cells in both groups of recipient mice (Fig. 6 E), demonstrating that the profound loss of LT-HSCs in *Evi1*$^{+/-}$ mice is attributed to cell-intrinsic mechanisms.

Evi1 heterozygosity causes specific abrogation of self-renewal capacity in ST- and LT-HSCs

To further characterize which subpopulation in HSPCs is most dependent on Evi1, we purified CD34$^+$ and Flk-2$^-$ CD34$^-$ LSK cells from *Evi1*$^{+/+}$ and *Evi1*$^{+/-}$ mice and compared their differentiation and self-renewal capacity in vitro and in vivo. First, to assess the effect of Evi1 heterozygosity on the biological functions of ST-HSCs/MPPs, we performed colony-forming assays in vitro using *Evi1*$^{+/+}$ and *Evi1*$^{+/-}$ CD34$^+$ LSK cells, which demonstrated no significant differences in the number and type of colonies (Fig. 7 A). Similarly, we found the capacity of *Evi1*$^{+/-}$ CD34$^+$ LSK cells to form colonies in the spleen 11 d after transplantation (CFU-spleen [CFU-S]) was also equivalent to that of WT littermates (Fig. 7 B), indicating Evi1 is dispensable for the regulation of the differentiation and proliferation capacity in ST-HSCs/MPPs. Moreover, to investigate the self-renewal ability of ST-HSCs/MPPs in vivo, we evaluated the short-term repopulating capacity of purified CD34$^+$ LSK cells using a CRA. At 2 wk after transplantation, we detected comparable frequencies of *Evi1*$^{+/+}$ and *Evi1*$^{+/-}$ CD34$^+$ LSK cell–derived myeloid and B cells (Fig. 7 C), suggesting that heterozygosity of Evi1 does not affect the engraftment and differentiation potential of ST-HSCs/MPPs in vivo. However, at later time points in the experiment, we found a moderate but significant decline in the percentage of donor-derived cells from *Evi1*$^{+/-}$ mice (Fig. 7 D). These data indicate that heterozygosity of Evi1 attenuates the self-renewal capacity of ST-HSCs/MPPs, but is not accompanied by any specific differentiation defects in them.

To assess whether Evi1 is required for the functions of LT-HSCs, we compared the self-renewal and proliferation capacity of *Evi1*$^{+/+}$ and *Evi1*$^{+/-}$ Flk-2$^-$ CD34$^-$ LSK cells when cultured in serum-free medium. *Evi1*$^{+/-}$ Flk-2$^-$ CD34$^-$ LSK cells showed comparable proliferation with WT cells for the first week of culture, but thereafter they exhibited pronouncedly impaired growth (Fig. 7 E). After incubation, a significantly lower proportion of cultured *Evi1*$^{+/-}$ Flk-2$^-$ CD34$^-$ LSK cells remained in the LSK fraction than those from *Evi1*$^{+/+}$ mice (Fig. 7 F). In addition, we observed a prominent reduction of hematopoietic colonies contained in cultured *Evi1*$^{+/-}$ Flk-2$^-$ CD34$^-$ LSK cells (Fig. 7 G). Besides, most of the colonies generated from cultured *Evi1*$^{+/-}$ Flk-2$^-$ CD34$^-$ LSK cells consisted of only CFU-GM. These data indicate that heterozygosity of Evi1 results in accelerated loss of HSPCs, leading to the inefficient expansion of their progeny. To evaluate the colony-forming capacity at the single cell level, *Evi1*$^{+/+}$ and *Evi1*$^{+/-}$ Flk-2$^-$ CD34$^-$ LSK cells were clonally sorted and cultured in serum-free medium. Evi1 heterozygosity diminished the colony-forming efficiency of clone-sorted Flk-2$^-$ CD34$^-$ LSK cells, and single *Evi1*$^{+/-}$ Flk-2$^-$ CD34$^-$ LSK cells generated smaller colonies compared with control cells (Fig. 7 H), which indicates that the disruption of Evi1 gene not only decreases the number of clonogenic HSCs but also impairs the functional output per cell.

To assess the repopulating capacity of *Evi1*$^{+/-}$ LT-HSCs in vivo, we performed a CRA using purified Flk-2$^-$ CD34$^-$ LSK cells from *Evi1*$^{+/+}$ and *Evi1*$^{+/-}$ mice. Notably, *Evi1*$^{+/-}$ Flk-2$^-$ CD34$^-$ LSK cells were almost unable to efficiently repopulate all mature lineages as well as stem and progenitor cells 16 wk after transplantation (Fig. 7, I and J), suggesting that LT-HSC function is critically dependent on Evi1 gene dosage. In a noncompetitive setting, although recipients of *Evi1*$^{+/+}$ and *Evi1*$^{+/-}$ Flk-2$^-$ CD34$^-$ LSK cells had similar survival after transplantation (not depicted), *Evi1*$^{+/-}$ Flk-2$^-$ CD34$^-$ LSK cells showed impaired engraftment (Fig. 7 K), suggesting that *Evi1*$^{+/-}$ HSCs were outcompeted by residual host HSCs. However, some of those recipients exhibited long-term multilineage reconstitution (Fig. 7 K and not depicted), confirming that the multipotent differentiation capacity is not abrogated in *Evi1*$^{+/-}$ mice. To further explore the competitive disadvantage of *Evi1*$^{+/-}$ HSCs, we transplanted WT BM cells into unirradiated *Evi1*$^{+/+}$ or *Evi1*$^{+/-}$ mice.

Published November 14, 2011

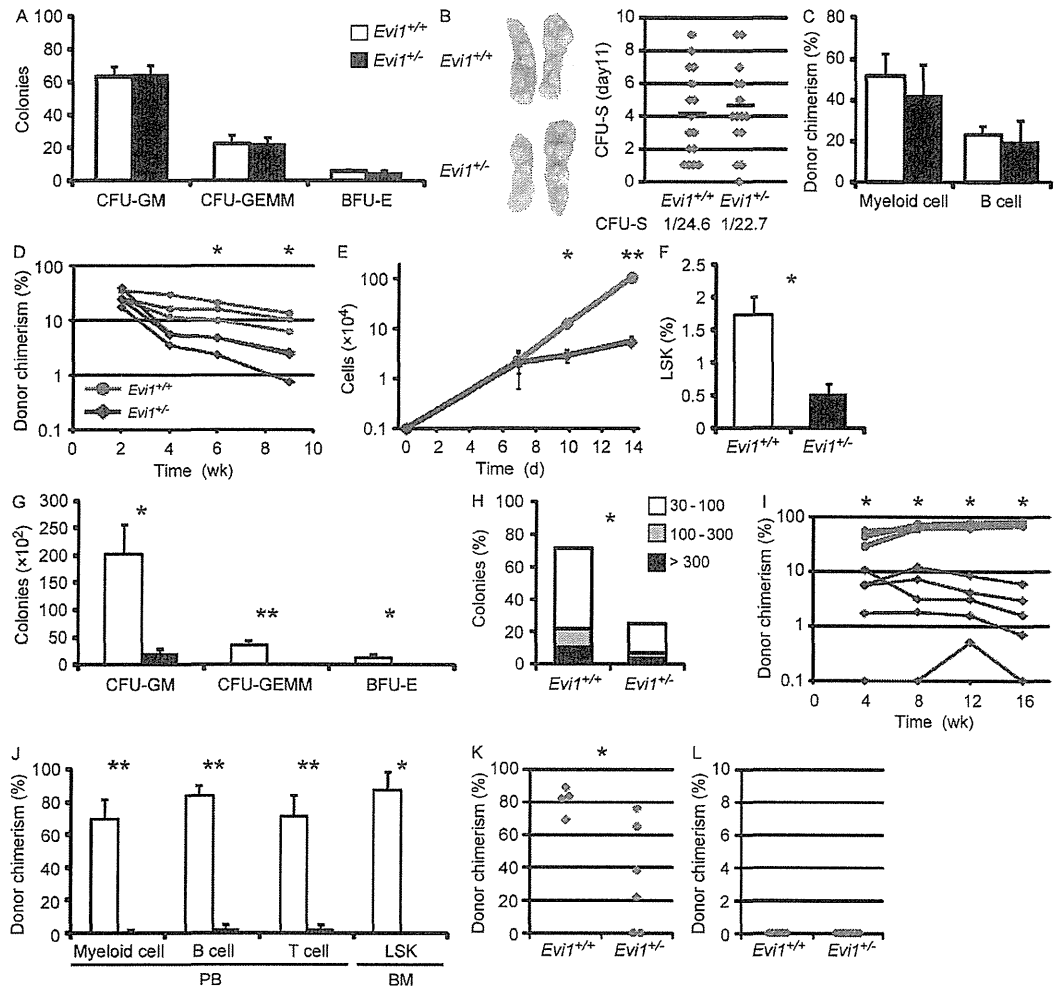

Figure 7. Evi1 heterozygosity causes specific abrogation of self-renewal capacity in ST- and LT-HSCs. (A) Numbers of CFU-GM, CFU-GEMM, and BFU-E colonies derived from 100 sorted *Evi1*$^{+/+}$ and *Evi1*$^{+/-}$ CD34$^+$ LSK cells ($n = 3$). (B) Appearance and number of CFU-S colonies in the spleen 11 d after injection of 100 sorted *Evi1*$^{+/+}$ or *Evi1*$^{+/-}$ CD34$^+$ LSK cells into lethally irradiated recipients. (left) Representative appearance is shown. (right) Data are shown as a dot plot and each bar represents mean ($n = 15$–16 from 3 independent experiments). (C and D) Short-term in vivo repopulating assay, in which 500 sorted *Evi1*$^{+/+}$ or *Evi1*$^{+/-}$ CD34$^+$ LSK cells (Ly5.2) were transplanted into lethally irradiated recipients (Ly5.1) together with 2×10^5 competitor BM cells (Ly5.1). (C) Percentages of donor-derived myeloid and B cells (Ly5.2) in PB 2 wk after transplantation are shown ($n = 3$). (D) Short-term kinetics of the percentages of donor-derived cells (Ly5.2) in PB. Each dot indicates an individual recipient mouse (*, $P < 0.05$; $n = 3$). (E) Proliferation of 1,000 sorted *Evi1*$^{+/+}$ and *Evi1*$^{+/-}$ Flk-2$^-$ CD34$^-$ LSK cells cultured in serum-free medium supplemented with 20 ng/ml SCF and 20 ng/ml TPO for 14 d (*, $P < 0.01$; ** $P < 0.001$; $n = 3$–4). (F) After 7 d of culture, the percentage of the remaining LSK fraction in cultured *Evi1*$^{+/+}$ and *Evi1*$^{+/-}$ Flk-2$^-$ CD34$^-$ LSK cells was analyzed (*, $P < 0.005$; $n = 3$). (G) In vitro colony-forming assay was performed to assess the numbers of CFU-GM, CFU-GEMM, and BFU-E colonies after 1,000 *Evi1*$^{+/+}$ and *Evi1*$^{+/-}$ Flk-2$^-$ CD34$^-$ LSK cells were cultured for 14 d (*, $P < 0.01$; ** $P < 0.001$; $n = 3$–4). (H) Single *Evi1*$^{+/+}$ and *Evi1*$^{+/-}$ Flk-2$^-$ CD34$^-$ LSK cells were clone-sorted and cultured in serum-free medium. After 14 d of culture, cell numbers in each colony were analyzed. Their relative distribution is shown (*, $P < 0.0001$; $n = 192$ clones from 2 independent experiments). (I–J) Long-term in vivo repopulating assay, in which 200 sorted *Evi1*$^{+/+}$ or *Evi1*$^{+/-}$ Flk-2$^-$ CD34$^-$ LSK cells (Ly5.2) were transplanted into lethally irradiated recipients (Ly5.1) together with 2×10^5 competitor BM cells (Ly5.1). (I) Percentages of donor-derived cells (Ly5.2) in PB after transplantation are shown. Each dot indicates an individual recipient mouse (*, $P < 0.0001$, $n = 5$–6). (J) Percentages of donor-derived cells (Ly5.2) in myeloid, B, and T cells of PB and LSK cells of BM 16 wk after transplantation (*, $P < 0.001$; ** $P < 0.0001$; $n = 5$–6 for PB and $n = 3$ for BM). (K) Noncompetitive repopulating assay, in which 200 sorted *Evi1*$^{+/+}$ or *Evi1*$^{+/-}$ Flk-2$^-$ CD34$^-$ LSK cells (Ly5.2) were transplanted into lethally irradiated recipients (Ly5.1) without competitor. Percentages of donor-derived cells (Ly5.2) in PB of recipient mice that survived 12 wk after transplantation are shown (*, $P < 0.05$, $n = 4$–6). (L) Reciprocal transplantation assay was performed by transplantation of 2×10^5 WT BM cells (Ly5.1) into unirradiated *Evi1*$^{+/+}$ or *Evi1*$^{+/-}$ mice (Ly5.2). Percentages of donor-derived cells (Ly5.1) in PB 16 wk after transplantation are shown ($n = 6$–8). Data represent mean ± SD.

Published November 14, 2011

JEM

We found no engraftment in both mice (Fig. 7 L), which indicates that the resistance to the donor HSC engraftment during steady-state hematopoiesis is maintained in *Evi1*$^{+/-}$ mice. Collectively, these data suggest that Evi1 is dispensable for the regulation of proliferative and differentiation capacity of ST-HSCs/MPPs, but is strictly required for the maintenance of LT-HSC activity.

To investigate the mechanism behind the impaired HSC activity, we performed cell-cycle and apoptosis assays, but found no differences in the cell-cycle profile or apoptotic rates of Flk-2$^-$ CD34$^-$ LSK cells between *Evi1*$^{+/+}$ and *Evi1*$^{+/-}$ mice (unpublished data). Collectively, in consideration of the accelerated loss of LT-HSC activity in *Evi1*$^{+/-}$ mice, it is supposed that Evi1 heterozygosity directs LT-HSCs from self-renewal toward differentiation to generate more committed progenitors, which is uncoupled from cell-cycle progression or apoptosis.

Forced expression of Evi1 prevents HSPC differentiation and enhances their expansion

The findings noted above led us to hypothesize Evi1 has the potential to inhibit differentiation and enhance HSC self-renewal independent of cell-cycle progression. To clarify this, we adopted a gain-of-function approach, in which WT LSK cells were transduced with Evi1, and then incubated in serum-free medium. Although forced expression of Evi1 gave no apparent growth advantage for the first 10 d of culture, Evi1-transduced LSK cells subsequently manifested a mild but significant increase in proliferation rate (Fig. 8 A). Moreover, we found a substantial increase in the frequency of the remaining LSK fraction in cultured Evi1-transduced cells compared with control cells (Fig. 8 B). In parallel, the number of colonies derived from cultured Evi1-transduced LSK cell was drastically increased (Fig. 8 C). These results suggest that Evi1 activation restricts lineage differentiation and enhances self-renewal activity of HSPCs. Collectively, our data provide compelling evidence that Evi1 regulates the developmental transition from HSPCs to more committed progenitors, suggesting a crucial role of Evi1 in controlling the balance between self-renewal and differentiation.

A recent work suggests that the longer, PR domain-containing isoform Mds1-Evi1 (ME) deficiency alone causes a reduction in the number of HSCs with a loss of long-term repopulation capacity (Zhang et al., 2011). Because both ME and Evi1 are inactivated in our *Evi1* KO model (Goyama et al., 2008), we attempted to genetically dissect the relative roles of ME and Evi1 in maintaining LT-HSCs. For this purpose, we transduced Evi1 or ME into *Evi1*$^{+/-}$ Flk-2$^-$ CD34$^-$ LSK cells and examined whether they could maintain stem cell phenotype after in vitro culture. Reintroduction of Evi1 led to a significant increase in the proportion that remained in the LSK fraction, similar to observations made in *Evi1*$^{+/+}$ cells (Fig. 8 D). However, retroviral transfer of ME was unable to normalize the frequency of the remaining LSK fraction (Fig. 8 D), indicating that Evi1 preferentially rescues *Evi1*$^{+/-}$ LT-HSC defects. Given that ME has broader effects on the hematopoietic system than Evi1 and acts in part by maintaining HSC quiescence through up-regulation of *Cdkn1c* transcription (Zhang et al., 2011), Evi1 and ME may exert their functions in regulating hematopoiesis at different stages and by different mechanisms.

DISCUSSION

In this study, we show that the amount of *Evi1* transcript can be indicative of an undifferentiated state with multipotent differentiation capacity within HSPCs. In both the fetal and adult hematopoietic systems, Evi1 expression can mark long-term multilineage repopulating HSCs, and enhance HSC purification with a combination of other surface markers, suggesting a specific relationship between HSC activity and Evi1 expression throughout ontogeny. This stem cell-specific expression pattern of Evi1 allows us to functionally identify self-renewing HSCs by using Evi1-IRES-GFP knock-in mice, and suggests the relevance of Evi1 in fine-tuning of stem cell properties. Indeed, we provide the genetic evidence confirming that Evi1 has a predominant effect on LT-HSCs by specifically regulating their self-renewal capacity.

The prospective isolation of HSCs is the most important step to dissect their function. The strategy commonly used for HSC isolation is purification based on the expression of a combination of cell surface markers. However, some of these parameters differ between strains of mice, change dramatically during development, and are expressed on many non-HSCs.

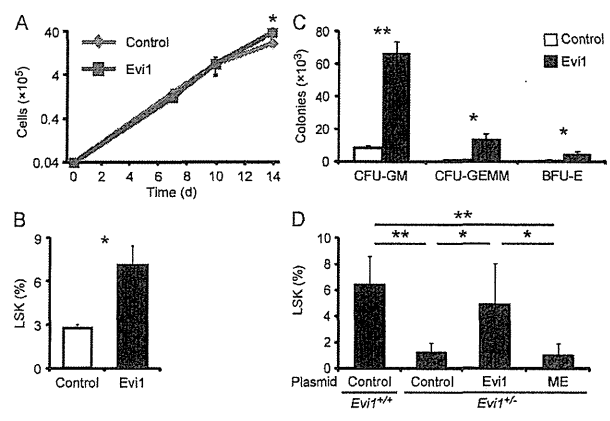

Figure 8. Forced expression of Evi1 prevents HSPC differentiation and promotes their expansion. (A) Proliferation of 3,000 control- or Evi1-transduced LSK cells cultured in serum-free medium with 20 ng/ml SCF and 20 ng/ml TPO for 14 d (*, $P < 0.05$; $n = 3$). (B) After 7 d of culture, the percentage of the remaining LSK fraction in cultured control- or Evi1-transduced LSK cells was analyzed (*, $P < 0.01$; $n = 3$). (C) In vitro colony-forming assay was performed to assess the numbers of CFU-GM, CFU-GEMM, and BFU-E colonies after 3,000 control- or Evi1-transduced LSK cells were cultured for 14 d (*, $P < 0.005$; **, $P < 0.0005$; $n = 3$). (D) Control-, Evi1-, or ME-transduced *Evi1*$^{+/+}$ or *Evi1*$^{+/-}$ Flk-2$^-$ CD34$^-$ LSK cells were cultured in medium containing 10% serum with 50 ng/ml SCF, 50 ng/ml TPO, 10 ng/ml IL-3, and 10 ng/ml IL-6 for 5 d, and the percentages of the remaining LSK fraction were analyzed (*, $P < 0.05$; **, $P < 0.0005$; $n = 5$–6). Data represent mean ± SD.

Published November 14, 2011

Here, we reveal that Evi1 expression specifically correlates with functional HSCs, whereas lack of Evi1 expression exclusively identifies cells without functional HSC activity in both the fetal and adult hematopoietic systems. In particular, Evi1 expression can segregate long-term repopulating HSCs from cells without self-renewal potential even within the highly subfractionated Flk-2$^-$ CD34$^-$ LSK or CD48$^-$ CD150$^+$ LSK compartments. In addition, Evi1-IRES-GFP knock-in mice offer advantages over the conventional HSC surface markers, as the GFP$^-$ and GFP$^+$ subfractions of the Flk-2$^-$ CD34$^-$ LSK or CD48$^-$ CD150$^+$ LSK cells show a quite similar distribution of these markers (unpublished data). Moreover, our findings that Evi1 specifically regulates the self-renewal capacity of HSCs guarantee the potential utility of Evi1 expression as an indicator of HSC activity. Therefore, the Evi1-IRES-GFP knock-in mouse line provides a powerful approach for the functional identification of self-renewing HSCs in vivo, thus opening a new avenue for investigating HSC biology.

Although functional HSCs exclusively reside in the GFP$^+$ population, a proportion of GFP$^+$ cells lack HSC function. As GFP protein is quite stable and degraded more slowly than Evi1 protein (unpublished data), these observations may reflect a remnant of GFP expression from cells that have just differentiated from GFP$^+$ HSCs. However, it is possible that Evi1 expression distinguishes self-renewing ST-HSCs from cells with no self-renewal activity in the ST-HSC/MPP fraction, as Evi1 heterozygosity affects the short-term repopulating capacity of CD34$^+$ LSK cells.

The present findings in the hematopoietic system encourage us to examine the possibility that Evi1 expression serves as a selective marker for stem cells in other tissues or in cancer systems. We show that mesenchymal stem cells (MSCs), one of the few tissue stem cell types that have been established to self-renew in vivo (Morikawa et al., 2009), do not express Evi1. However, a mouse gene expression atlas and prior studies examining the expression pattern of Evi1 in various tissues have reported Evi1 expression in the kidney, ovary, uterus, intestine, stomach, lung, trachea, and nasal cavity in the adult mouse (Morishita et al., 1990; Perkins et al., 1991; Su et al., 2004). It will be interesting to determine, using Evi1-IRES-GFP knock-in mice, whether Evi1-expressing cells in these organs are enriched with tissue stem cells.

Our data suggest a unique association between Evi1 expression and HSC self-renewal activity throughout hematopoietic ontogeny. Along with this stem cell–specific expression pattern of Evi1, the fact that the disruption of a single allele of Evi1 leads to a near total loss of self-renewing HSCs implicates Evi1 as a central regulator in HSC self-renewal. In addition, a recent gene expression profile analysis showed that Evi1 binding sites are enriched in the upstream region of genes expressed selectively in LT-HSCs (Forsberg et al., 2010). In fact, several molecules involved in the regulation of HSC self-renewal have been identified as downstream targets or interacting proteins of Evi1, including Gata2 (Sato et al., 2008; Yuasa et al., 2005), Pbx1 (Shimabe et al., 2009), Runx1 (Senyuk et al., 2007), and TGF-β (Kurokawa et al., 1998). Together with these findings, our data strongly support a model in which Evi1 gene dosage is a critical determinant of HSC self-renewal potential.

Inappropriate expression of EVI1 confers poor prognosis in patients with AML (Lugthart et al., 2008; Gröschel et al., 2010), and therefore improvement of the therapeutic outcome of leukemia with high EVI1 expression is needed. In this study, we reveal that Evi1 overexpression blocks differentiation and induces HSPC expansion. Our data fit with other studies showing that retroviral integration at the *Evi1* locus can be associated with long-term in vivo clonal dominance, occasionally leading to leukemic transformation (Stein et al., 2010). The genetic events underlying AML pathogenesis fall into two groups: (1) mutations that enhance proliferation and survival of hematopoietic progenitors, or (2) mutations that result in impaired differentiation or aberrant acquisition of self-renewal properties of HSPCs (Fröhling et al., 2005). Our data indicate that Evi1 activation can function as the latter mutation and confer enhanced self-renewal capacity in myeloid neoplasms. In addition, we demonstrate that retroviral transfer of Evi1, but not ME, can ameliorate the self-renewal defects in *Evi1*$^{+/-}$ HSCs, highlighting a distinct role of Evi1 in HSC self-renewal. These findings may explain the underlying mechanisms of the clinical observations that, irrespective of ME expression, aberrant EVI1 expression carries an adverse prognostic value in AML (Lugthart et al., 2008, 2010). As it is becoming evident that leukemic stem cells share self-renewal machinery with normal HSCs, the elucidation of how Evi1 controls HSC self-renewal may provide biological insight into the pathogenesis of Evi1-related leukemia.

MATERIALS AND METHODS

Generation of Evi1-IRES-GFP knock-in mice. The targeting construct was assembled in the plasmid vector pBluescript KS. The 5′ arm of the targeting vector consists of a 5.1-kb fragment of BAC clone RP24-481A14 and the 3′ arm consists of a 3.1-kb fragment. The 5′ arm contains *Evi1* intron 8 and exon 9, and the 3′ arm contains intron 9, exon 10, and intron 10. Both arms were obtained by PCR using BAC clone RP24-481A14 as a template, all sequenced, and then inserted into pBluescript KS. Mouse *Evi1* cDNA was isolated from murine embryo cDNA by PCR, with an EcoRI site at the 5′ end and a BamHI site at the 3′ end, which was cloned into pBluescript KS. A 1.3-kb IRES-GFP cassette derived from pGCDNsam-IRES-GFP retroviral vector was inserted downstream of the aforementioned *Evi1* fragment. A polyadenylation (pA) cassette was then ligated 3′ to the IRES-GFP cassette. A neomycin-positive selection (Neo^r) cassette, expressed under control of the PGK promoter, was inserted downstream of the pA cassette. Both pA cassette and loxP-flanked neomycin-positive selection cassette were derived from DT-A/AFP(EGFP)/Neo vector (a gift from the Institute of Physical and Chemical Research Center for Developmental Biology, Kobe, Japan). The partial *Evi1 cDNA-IRES-GFP-pA-loxP-neo* was released intact by digestion with *Sse*8387I and cloned into a unique *Sse*8387I site in exon 9 of BAC arm. A diphtheria toxin–negative selection cassette was cloned into pBluescript KS, 3′ to the targeting construct. The targeting construct was linearized by SacII and transfected into TT2 ES cells by electroporation. Homologous recombinant clones were identified by Southern blot analysis of genomic DNA isolated from individual G418/FIAU-resistant ES cell colonies. The DNA was digested with XbaI, blotted to nylon membranes, and

Published November 14, 2011

JEM

hybridized with a 3′ external *Evi1* probe. Confirmatory Southern blotting could detect a 9.1-kb WT *Evi1* allele band and a 4.1-kb correctly targeted *Evi1-IRES-GFP* allele band with this 3′ probe. In EcoRV-digested genomic DNA from positive ES cell clones, a 5′ external probe detected 10- and 11-kb bands from the WT and targeted alleles, respectively. Next, appropriately targeted ES clones were aggregated with 8-cell stage of ICR embryo, and resultant blastocysts were injected into pseudopregnant foster ICR mothers. Chimeric males, which gave germ-line transmission, were crossed with C57BL/6 females. Blastocyst injection and breeding of chimeras were performed in the Animal Center for Biomedical Research, University of Tokyo, Tokyo, Japan.

Mice. Evi1-IRES-GFP knock-in mice were backcrossed onto a C57BL/6 background (Ly5.1 or Ly5.2) for at least four generations (Sankyo-Laboratory Service). Heterozygous *Evi1* KO mice (*Evi1*$^{+/-}$ mice) were previously described (Goyama et al., 2008). C57BL/6-Ly5.1 mice were crossed with Ly5.2 mice to obtain Ly5.1/Ly5.2 mice. Littermates were used as controls in all experiments. All animal experiments were approved by the University of Tokyo Ethics Committee for Animal Experiments and strictly adhered to the guidelines for animal experiments of the University of Tokyo.

Genotype analysis. *Evi1*$^{+/-}$ mice were genotyped by PCR as previously described (Goyama et al., 2008). *Evi1*$^{+/GFP}$ mice were genotyped using a multiplex PCR to detect both WT and *Evi1-IRES-GFP* alleles. Genomic DNA was isolated from tail biopsies and subjected to PCR using *Neo* and *Evi1* primers. PCR with *Neo* primers detects the knock-in allele, and that with *Evi1* primers detects the WT allele. The PCR samples were denatured at 94°C for 2 min, subjected to 30 cycles of amplification (94°C for 30 s, 65°C for 1 min, and 72°C for 1 min), and followed by a final extension step at 72°C. PCR products were resolved by agarose gel electrophoresis. PCR primers are listed below: *Neo* primer forward, 5′-AGGGGATCCGCTGTAAGTCT-3′, reverse, 5′-GCACTGACTGCTCATCCAAA-3′; *Evi1* primer forward, 5′-ATGTCAGCAATTGAGAACATGG-3′, reverse, 5′-ATCCAAAGGTCCTGAGTTCAAA-3′.

Flow cytometry. A list of antibodies is provided in Table S1. Stained cells were sorted with a FACSAriaII, and analysis was performed on LSRII (both from BD). A mixture of antibodies recognizing CD3, CD4, CD8, B220, TER-119, Mac-1, or Gr-1 was used to identify Lin$^+$ cells. Anti-CD127 antibody was added to the lineage mixture, except for the analysis of CLPs. The data analyses were performed with FlowJo software (Tree Star). In experiments with the Evi1-IRES-GFP knock-in mouse, a "fluorescence minus one" littermate control was analyzed in parallel to set GFP gates.

Cell-cycle analyses. For Hoechst 33342 and pyronin Y staining, cells were incubated with 5 ng/ml Hoechst 33342 (Invitrogen) and 25 μg/ml verapamil at 37°C for 45 min. Next, pyronin Y (Sigma-Aldrich) was added to 1 μg/ml, and the cells were incubated for an additional 15 min.

In vitro culture. For in vitro serum-free culture, cells were cultured in StemSpan SFEM (StemCell Technologies) supplemented with 20 ng/ml mouse SCF and 20 ng/ml human TPO, and subsequently subjected to flow cytometry or colony-forming assay at the indicated day after incubation. For colony-forming assay, cells were seeded in duplicate and cultured in cytokine-supplemented methylcellulose medium (MethoCult GF M3434; Stem Cell Technologies). Subsequently, colonies were counted and identified based on morphological examination on day 12. For in vitro differentiation, LSK GFP$^+$ cells were cultured in RPMI-1640 medium (Wako) containing 10% serum with 50 ng/ml mouse SCF, 50 ng/ml human TPO, 10 ng/ml mouse IL-3, and 10 ng/ml human IL-6, and subjected to flow cytometry or colony-forming assay after 5 d of incubation.

Single-cell culture. Cells were clone-sorted into 96-well plates using FACS-based automated cell deposition unit and cultured in StemSpan SFEM supplemented with 20 ng/ml mouse SCF and 20 ng/ml human TPO. After 14 d of culture, cell numbers in each colony were analyzed.

In vivo transplantation assay. Transplantation assays were performed using the Ly5 congenic mouse system. In CRAs, lethally irradiated (9.5 Gy) mice were reconstituted with the indicated subsets from *Evi1*$^{+/+}$, *Evi1*$^{+/GFP}$, or *Evi1*$^{+/-}$ mice, in competition with 2×10^5 unfractionated BM cells from congenic mice. For second BM transplantation, BM cells (1/2 femur equivalent) were obtained from recipient mice 16 wk after transplantation, and transplanted into a second set of lethally irradiated (9.5 Gy) mice. For reciprocal transplantation assays, lethally irradiated (9.5 Gy) or unirradiated *Evi1*$^{+/+}$ and *Evi1*$^{+/-}$ mice were transplanted with 2×10^5 WT BM cells without competitor cells. In non-CRAs, lethally irradiated (9.5 Gy) mice were reconstituted with *Evi1*$^{+/+}$ and *Evi1*$^{+/-}$ Flk-2$^-$ CD34$^-$ LSK cells without competitor cells. Reconstitution of donor-derived cells was monitored by staining PB cells with antibodies against Ly5.1, Ly5.2, CD3, CD4, CD8, B220, Mac-1, and Gr-1. When CD48$^+$ CD150$^-$ LSK cells were transplanted, nonblocking anti-CD48 antibody (MRC OX78 clone) was used (Grassinger et al., 2010).

CFU-S assay. For CFU-S assay, 100 CD34$^+$ LSK cells were injected into lethally irradiated (9.5 Gy) mice. Spleens in transplanted mice were isolated 11 d later, and visually inspected for the presence of macroscopic colonies after fixation in Tellyesniczky's solution.

RQ-PCR. Total RNA was prepared using RNeasy Mini kit (QIAGEN), then cDNA was synthesized with a QuantiTect Reverse Transcription kit (QIAGEN), and used for RQ-PCR with FastStart SYBR Green Master and LightCycler 480 System (Roche Applied Science) according to the manufacturer's instructions. All assays were performed in triplicate and relative expression was normalized to the internal control *GAPDH*. PCR primers are listed below: *GAPDH* primer forward, 5′-CCATCACCATCTTCCAGGAG-3′, reverse, 5′-CCTGCTTCACCACCTTCTTG-3′; *Evi1* primer forward, 5′-ATCGGAAGATCTTAGATGAGTTTTG-3′, reverse, 5′-CTTCCTACATCTGGTTGACTGG-3′

Western blotting. Western blotting was performed as previously described (Goyama et al., 2008). In brief, mouse embryo fibroblast cells were lysed in TNE buffer, subjected to 7% SDS-PAGE, and transferred to a PVDF membrane (Millipore). The blot was incubated with an Evi-1 (C50E12) rabbit monoclonal antibody (Cell Signaling Technology), and visualized by ECL Plus (GE Healthcare).

AGM and placental cell preparation. The day of vaginal plug observation was considered as day 0.5 postcoitum (E0.5). E10.5 AGM region or E12.5 placenta were carefully dissected from embryos, dissociated by incubation with 250 U/ml dispase (Godo Shusei) for 20 min and cell dissociation buffer (Invitrogen) for 20 min at 37°C, and followed by passages through 18–25 G needles. Single cell suspensions were filtered through 70-μm cell strainer and analyzed by flow cytometry.

Endothelial cell (EC), osteoblast (OB), and MSC preparation. After BM cells were flushed out, bones were crushed with a pestle and mortar. Then bone fragments were incubated with a Collagenase/Dispase (1 mg/ml; Roche Applied Science) in MEM α (Wako) with 20% serum and gently agitated for 90 min at 37°C. The dissociated cells were collected, and bone-associated mononuclear cells were isolated with the use of density centrifugation with Histopaque-1083 (Sigma-Aldrich). ECs were defined as CD31$^+$ TER-119$^-$ CD45$^-$, OBs were defined as CD31$^-$ TER-119$^-$ CD45$^-$ Sca-1$^-$ ALCAM$^+$ cells (Nakamura et al., 2010), and MSCs were defined as CD31$^-$ TER-119$^-$ CD45$^-$ Sca-1$^+$ PDGFRα$^+$ cells (Morikawa et al., 2009).

Plasmid construct and retroviral transduction of LSK cells. The murine *Evi1* or *ME* cDNA were inserted into a site upstream of an IRES-EGFP cassette in the retroviral vector pGCDNsam. To produce Evi1-GFP–expressing retrovirus, Plat-E packaging cells were transiently transfected with retroviral constructs by using FuGENE 6 transfection reagent (Roche). LSK cells were purified and incubated in StemSpan SFEM medium and cytokines (100 ng/ml mouse SCF and 100 ng/ml human TPO) for 24 h.

Published November 14, 2011

Next, cultured LSK cells were infected with Evi1-GFP retrovirus in the presence of RetroNectin (Takara Bio Inc.). The infected LSK cells were harvested 36 h after retrovirus infection, and GFP$^+$ cells were sorted and subjected to in vitro culture. For retroviral transduction of Evi1 or ME into *Evi1*$^{+/+}$ and *Evi1*$^{+/-}$ Flk-2$^-$ CD34$^-$ LSK cells, those cells were sorted and immediately infected with Evi1- or ME-GFP retroviruses in the presence of RetroNectin. These cells were incubated in RPMI-1640 medium containing 10% serum and cytokines (50 ng/ml mouse SCF, 50 ng/ml human TPO, 10 ng/ml mouse IL-3, and 10 ng/ml human IL-6). After 5 d of culture, the percentage of the remaining LSK fraction in GFP$^+$ cells was analyzed by flow cytometry.

Statistical analysis. Statistical significance of differences between parameters was assessed using a two-tailed unpaired Student's *t* test or Wilcoxon rank sum test.

Online supplemental material. Fig. S1 shows FACS gating strategy used to identify GFP$^+$ population from adult BM of *Evi1*$^{+/GFP}$ mice. Fig. S2 shows FACS gating strategy used to identify GFP$^+$ population from E12.5 placenta or E14.5 FL of *Evi1*$^{+/GFP}$ embryos. Table S1 lists the antibodies used for flow cytometry. Online supplemental material is available at http://www.jem.org/cgi/content/full/jem.20110447/DC1.

We thank T. Kitamura for Plat-E packaging cells; H. Nakauchi and M. Onodera for pGCDNsam-IRES-EGFP retroviral vector; Y. Shimamura, Y. Sawamoto, R. Takizawa, and Y. Oikawa for expert technical assistance; and Institute of Physical and Chemical Research Center for Developmental Biology for DT-A/AFP(EGFP)/Neo plasmid.

This work was supported in part by a Grant-in-Aid for Scientific Research from the Japan Society for the Promotion of Science and by Health and Labour Sciences Research grants from the Ministry of Health, Labour and Welfare. K. Kataoka is a Research Fellow of the Japan Society for the Promotion of Science.

The authors have no conflicting financial interests.

Submitted: 1 March 2011
Accepted: 14 October 2011

REFERENCES

Akashi, K., X. He, J. Chen, H. Iwasaki, C. Niu, B. Steenhard, J. Zhang, J. Haug, and L. Li. 2003. Transcriptional accessibility for genes of multiple tissues and hematopoietic lineages is hierarchically controlled during early hematopoiesis. *Blood.* 101:383–389. http://dx.doi.org/10.1182/blood-2002-06-1780

Bowie, M.B., K.D. McKnight, D.G. Kent, L. McCaffrey, P.A. Hoodless, and C.J. Eaves. 2006. Hematopoietic stem cells proliferate until after birth and show a reversible phase-specific engraftment defect. *J. Clin. Invest.* 116:2808–2816. http://dx.doi.org/10.1172/JCI28310

Buonamici, S., D. Li, Y. Chi, R. Zhao, X. Wang, L. Brace, H. Ni, Y. Saunthararajah, and G. Nucifora. 2004. EVI1 induces myelodysplastic syndrome in mice. *J. Clin. Invest.* 114:713–719.

Chen, W., A.R. Kumar, W.A. Hudson, Q. Li, B. Wu, R.A. Staggs, E.A. Lund, T.N. Sam, and J.H. Kersey. 2008. Malignant transformation initiated by Mll-AF9: gene dosage and critical target cells. *Cancer Cell.* 13:432–440. http://dx.doi.org/10.1016/j.ccr.2008.03.005

Forsberg, E.C., E. Passegué, S.S. Prohaska, A.J. Wagers, M. Koeva, J.M. Stuart, and I.L. Weissman. 2010. Molecular signatures of quiescent, mobilized and leukemia-initiating hematopoietic stem cells. *PLoS ONE.* 5:e8785. http://dx.doi.org/10.1371/journal.pone.0008785

Fröhling, S., C. Scholl, D.G. Gilliland, and R.L. Levine. 2005. Genetics of myeloid malignancies: pathogenetic and clinical implications. *J. Clin. Oncol.* 23:6285–6295. http://dx.doi.org/10.1200/JCO.2005.05.010

Goyama, S., and M. Kurokawa. 2009. Pathogenetic significance of ecotropic viral integration site-1 in hematological malignancies. *Cancer Sci.* 100:990–995. http://dx.doi.org/10.1111/j.1349-7006.2009.01152.x

Goyama, S., G. Yamamoto, M. Shimabe, T. Sato, M. Ichikawa, S. Ogawa, S. Chiba, and M. Kurokawa. 2008. Evi-1 is a critical regulator for hematopoietic stem cells and transformed leukemic cells. *Cell Stem Cell.* 3:207–220. http://dx.doi.org/10.1016/j.stem.2008.06.002

Grassinger, J., D.N. Haylock, B. Williams, G.H. Olsen, and S.K. Nilsson. 2010. Phenotypically identical hemopoietic stem cells isolated from different regions of bone marrow have different biologic potential. *Blood.* 116:3185–3196. http://dx.doi.org/10.1182/blood-2009-12-260703

Gröschel, S., S. Lugthart, R.F. Schlenk, P.J. Valk, K. Eiwen, C. Goudswaard, W.J. van Putten, S. Kayser, L.F. Verdonck, M. Lübbert, et al. 2010. High EVI1 expression predicts outcome in younger adult patients with acute myeloid leukemia and is associated with distinct cytogenetic abnormalities. *J. Clin. Oncol.* 28:2101–2107. http://dx.doi.org/10.1200/JCO.2009.26.0646

Kiel, M.J., O.H. Yilmaz, T. Iwashita, O.H. Yilmaz, C. Terhorst, and S.J. Morrison. 2005. SLAM family receptors distinguish hematopoietic stem and progenitor cells and reveal endothelial niches for stem cells. *Cell.* 121:1109–1121. http://dx.doi.org/10.1016/j.cell.2005.05.026

Kim, I., S. He, O.H. Yilmaz, M.J. Kiel, and S.J. Morrison. 2006. Enhanced purification of fetal liver hematopoietic stem cells using SLAM family receptors. *Blood.* 108:737–744. http://dx.doi.org/10.1182/blood-2005-10-4135

Kurokawa, M., K. Mitani, K. Irie, T. Matsuyama, T. Takahashi, S. Chiba, Y. Yazaki, K. Matsumoto, and H. Hirai. 1998. The oncoprotein Evi-1 represses TGF-beta signalling by inhibiting Smad3. *Nature.* 394:92–96. http://dx.doi.org/10.1038/27945

Lugthart, S., E. van Drunen, Y. van Norden, A. van Hoven, C.A. Erpelinck, P.J. Valk, H.B. Beverloo, B. Löwenberg, and R. Delwel. 2008. High EVI1 levels predict adverse outcome in acute myeloid leukemia: prevalence of EVI1 overexpression and chromosome 3q26 abnormalities underestimated. *Blood.* 111:4329–4337. http://dx.doi.org/10.1182/blood-2007-10-119230

Lugthart, S., S. Gröschel, H.B. Beverloo, S. Kayser, P.J. Valk, S.L. van Zelderen-Bhola, G. Jan Ossenkoppele, E. Vellenga, E. van den Berg-de Ruiter, U. Schanz, et al. 2010. Clinical, molecular, and prognostic significance of WHO type inv(3)(q21q26.2)/t(3;3)(q21;q26.2) and various other 3q abnormalities in acute myeloid leukemia. *J. Clin. Oncol.* 28:3890–3898. http://dx.doi.org/10.1200/JCO.2010.29.2771

McKinney-Freeman, S.L., O. Naveiras, F. Yates, S. Loewer, M. Philitas, M. Curran, P.J. Park, and G.Q. Daley. 2009. Surface antigen phenotypes of hematopoietic stem cells from embryos and murine embryonic stem cells. *Blood.* 114:268–278. http://dx.doi.org/10.1182/blood-2008-12-193888

Mikkola, H.K., and S.H. Orkin. 2006. The journey of developing hematopoietic stem cells. *Development.* 133:3733–3744. http://dx.doi.org/10.1242/dev.02568

Morikawa, S., Y. Mabuchi, Y. Kubota, Y. Nagai, K. Niibe, E. Hiratsu, S. Suzuki, C. Miyauchi-Hara, N. Nagoshi, T. Sunabori, et al. 2009. Prospective identification, isolation, and systemic transplantation of multipotent mesenchymal stem cells in murine bone marrow. *J. Exp. Med.* 206:2483–2496. http://dx.doi.org/10.1084/jem.20091046

Morishita, K., E. Parganas, D.M. Parham, T. Matsugi, and J.N. Ihle. 1990. The Evi-1 zinc finger myeloid transforming gene is normally expressed in the kidney and in developing oocytes. *Oncogene.* 5:1419–1423.

Nakamura, Y., F. Arai, H. Iwasaki, K. Hosokawa, I. Kobayashi, Y. Gomei, Y. Matsumoto, H. Yoshihara, and T. Suda. 2010. Isolation and characterization of endosteal niche cell populations that regulate hematopoietic stem cells. *Blood.* 116:1422–1432. http://dx.doi.org/10.1182/blood-2009-08-239194

Orford, K.W., and D.T. Scadden. 2008. Deconstructing stem cell self-renewal: genetic insights into cell-cycle regulation. *Nat. Rev. Genet.* 9:115–128. http://dx.doi.org/10.1038/nrg2269

Orkin, S.H., and L.I. Zon. 2008. Hematopoiesis: an evolving paradigm for stem cell biology. *Cell.* 132:631–644. http://dx.doi.org/10.1016/j.cell.2008.01.025

Perkins, A.S., J.A. Mercer, N.A. Jenkins, and N.G. Copeland. 1991. Patterns of Evi-1 expression in embryonic and adult tissues suggest that Evi-1 plays an important regulatory role in mouse development. *Development.* 111:479–487.

Ramalho-Santos, M., S. Yoon, Y. Matsuzaki, R.C. Mulligan, and D.A. Melton. 2002. "Stemness": transcriptional profiling of embryonic and adult stem cells. *Science.* 298:597–600. http://dx.doi.org/10.1126/science.1072530

Sato, T., S. Goyama, E. Nitta, M. Takeshita, M. Yoshimi, M. Nakagawa, M. Kawazu, M. Ichikawa, and M. Kurokawa. 2008. Evi-1 promotes

Published November 14, 2011

JEM

para-aortic splanchnopleural hematopoiesis through up-regulation of GATA-2 and repression of TGF-b signaling. *Cancer Sci.* 99:1407–1413. http://dx.doi.org/10.1111/j.1349-7006.2008.00842.x

Senyuk, V., K.K. Sinha, D. Li, C.R. Rinaldi, S. Yanamandra, and G. Nucifora. 2007. Repression of RUNX1 activity by EVI1: a new role of EVI1 in leukemogenesis. *Cancer Res.* 67:5658–5666. http://dx.doi.org/10.1158/0008-5472.CAN-06-3962

Shimabe, M., S. Goyama, N. Watanabe-Okochi, A. Yoshimi, M. Ichikawa, Y. Imai, and M. Kurokawa. 2009. Pbx1 is a downstream target of Evi-1 in hematopoietic stem/progenitors and leukemic cells. *Oncogene.* 28:4364–4374. http://dx.doi.org/10.1038/onc.2009.288

Stein, S., M.G. Ott, S. Schultze-Strasser, A. Jauch, B. Burwinkel, A. Kinner, M. Schmidt, A. Krämer, J. Schwäble, H. Glimm, et al. 2010. Genomic instability and myelodysplasia with monosomy 7 consequent to EVI1 activation after gene therapy for chronic granulomatous disease. *Nat. Med.* 16:198–204. http://dx.doi.org/10.1038/nm.2088

Su, A.I., T. Wiltshire, S. Batalov, H. Lapp, K.A. Ching, D. Block, J. Zhang, R. Soden, M. Hayakawa, G. Kreiman, et al. 2004. A gene atlas of the mouse and human protein-encoding transcriptomes. *Proc. Natl. Acad. Sci. USA.* 101:6062–6067. http://dx.doi.org/10.1073/pnas.0400782101

Takakura, N., T. Watanabe, S. Suenobu, Y. Yamada, T. Noda, Y. Ito, M. Satake, and T. Suda. 2000. A role for hematopoietic stem cells in promoting angiogenesis. *Cell.* 102:199–209. http://dx.doi.org/10.1016/S0092-8674(00)00025-8

Weksberg, D.C., S.M. Chambers, N.C. Boles, and M.A. Goodell. 2008. CD150- side population cells represent a functionally distinct population of long-term hematopoietic stem cells. *Blood.* 111:2444–2451. http://dx.doi.org/10.1182/blood-2007-09-115006

Yuasa, H., Y. Oike, A. Iwama, I. Nishikata, D. Sugiyama, A. Perkins, M.L. Mucenski, T. Suda, and K. Morishita. 2005. Oncogenic transcription factor Evi1 regulates hematopoietic stem cell proliferation through GATA-2 expression. *EMBO J.* 24:1976–1987. http://dx.doi.org/10.1038/sj.emboj.7600679

Zhang, Y., S. Stehling-Sun, K. Lezon-Geyda, S.C. Juneja, L. Coillard, G. Chatterjee, C.A. Wuertzer, F. Camargo, and A.S. Perkins. 2011. PR domain-containing Mds1-Evi1 is critical for long-term hematopoietic stem cells function. *Blood.* 118:3856–3861.

AML1/RUNX1 functions as a cytoplasmic attenuator of NF-κB signaling in the repression of myeloid tumors

Masahiro Nakagawa,[1] Munetake Shimabe,[1] Naoko Watanabe-Okochi,[1] Shunya Arai,[1] Akihide Yoshimi,[1] Akihito Shinohara,[1] Nahoko Nishimoto,[1] Keisuke Kataoka,[1] Tomohiko Sato,[1] Keiki Kumano,[1] Yasuhito Nannya,[1] Motoshi Ichikawa,[1] Yoichi Imai,[1] and Mineo Kurokawa[1]

[1]Department of Hematology and Oncology, Graduate School of Medicine, University of Tokyo, Tokyo, Japan

Functional deregulation of transcription factors has been found in many types of tumors. Transcription factor AML1/RUNX1 is one of the most frequent targets of chromosomal abnormalities in human leukemia and altered function of AML1 is closely associated with malignant transformation of hematopoietic cells. However, the molecular basis and therapeutic targets of AML1-related leukemia are still elusive. Here, we explored immediate target pathways of AML1 by in vitro synchronous inactivation in hematopoietic cells. We found that AML1 inhibits NF-κB signaling through interaction with IκB kinase complex in the cytoplasm. Remarkably, AML1 mutants found in myeloid tumors lack the ability to inhibit NF-κB signaling, and human cases with AML1-related leukemia exhibits distinctly activated NF-κB signaling. Furthermore, inhibition of NF-κB signaling in leukemic cells with mutated AML1 efficiently blocks their growth and development of leukemia. These findings reveal a novel role for AML1 as a cytoplasmic attenuator of NF-κB signaling and indicate that NF-κB signaling is one of the promising therapeutic targets of hematologic malignancies with AML1 abnormality. (*Blood.* 2011; 118(25):6626-6637)

Introduction

Functional disruption of tumor-suppressive transcription factors, such as p53, has been widely found in many types of tumors. Although great efforts have been made to reactivate wild-type p53,[1] therapeutic interventions to impaired transcription factors still need innovative strategy. To overcome this difficulty, we need to seek the treatable and pathogenetic targets for deregulated transcription factors.

Transcription factor AML1, also known as RUNX1, is one of the most frequent targets of chromosomal abnormalities in human leukemia.[2] Functional impairment of AML1 caused by point mutation also is reported in patients with leukemia or myelodysplastic syndrome (MDS).[3-6] Patients who have *AML1* mutations are reported to be accompanied with poor prognosis.[5,6] Genetic disruptions of *AML1* also are known to cause familial platelet disorder, with predisposition to acute myelogenous leukemia (AML).[7] AML1 is a critical regulator in hematopoiesis and has an essential function in the establishment of definitive hematopoiesis, differentiation of lymphocytes, maturation of megakaryocytes, and regulation of hematopoietic stem cells (HSCs).[8-11] Point mutations of *AML1* have been found throughout the length of this gene in myeloid tumors such as AML or MDS; most of the mutants loose the potential to activate gene transcription, whereas some mutants show a dominant-negative effect over AML1 function.[4,12] The types of mutations are similar between AML and MDS. Significantly, it was recently reported that AML1 mutants cause MDS/AML in a mouse bone marrow transplantation (BMT) model.[13] To date, many target genes of AML1 have been reported.[14,15] However, the signaling pathways involved in the pathogenesis of AML1-related leukemia are still elusive.

t(8;21) produces the chimeric protein AML1/ETO and is one of the most frequent chromosomal translocations found in AML. AML1/ETO is constituted of the N-terminal AML1-derived part and the C-terminal ETO part that contain a DNA-binding domain and a corepressor-binding domain, respectively. Besides the defect of trans-activation potential, AML1/ETO is a potent repressor of gene transcription and acts as a dominant-negative mutant of AML1.

Nuclear factor-κB is a dimeric complex of transcription factors mainly consisting of p65 (RelA)/p50 (NFKB1) or RelB/p52 (NFKB2). There are 2 major pathways in NF-κB signaling: the canonical pathway that broadly modulates cell proliferation, survival, or inflammation; and the noncanonical pathway that mainly controls lymphogenesis or B-cell maturation.[16] In the canonical pathway, p65 and p50 (NFKB1) constitute NF-κB complex and are localized in the cytoplasm with IκB in a steady state. Once inflammation is induced, TNF-α stimulates its receptor that in turn activates the IκB kinase (IKK) complex. Then, IκB is phosphorylated by the activated IKK complex and subsequently degraded through the ubiquitin-proteasome pathway, resulting in nuclear translocation of p65/p50 and transactivation of NF-κB target genes. In the noncanonical pathway, RelB stably binds to p100 (NFKB2) in the cytoplasm. During the maturation of B cells, B cell–activating factor of the TNF family (BAFF) stimulates its receptor and activates IKK complex that phosphorylates and processes p100 to p52, resulting in nuclear translocation.[17] Although these

Submitted December 22, 2010; accepted October 5, 2011. Prepublished online as *Blood* First Edition paper, October 21, 2011; DOI 10.1182/blood-2010-12-326710.

The online version of the article contains a data supplement.

The publication costs of this article were defrayed in part by page charge payment. Therefore, and solely to indicate this fact, this article is hereby marked "advertisement" in accordance with 18 USC section 1734.

2 pathways usually act in distinct physiologic conditions, their regulations are closely related, as indicated by the fact that transcriptional control of NFKB2 is directly regulated by p65.[18] Recently, deregulated activation of NF-κB signaling has been reported to be responsible for many types of tumors, including hematologic malignancies.[19-22]

In this study, we revealed that AML1 represses NF-κB signaling in the hematopoietic cells. This repression is achieved by inhibition of the kinase activity of IKK through physical interaction between AML1 and IKK. Remarkably, aberrant activation of NF-κB signaling is induced not only by targeted disruption but also by leukemia-related gene alteration of *AML1*. Furthermore, we demonstrate that blocking the NF-κB signaling efficiently represses proliferation of leukemic cells with mutant AML1, including chimeric proteins, and development of AML1-related leukemia in mice.

Methods

Mice

AML1 cKO mice were described previously.[11] Homozygous AML1 floxed mice (AML1 f/f) and Mx-Cre–expressing homozygous AML1 floxed mice [AML1 f/f Mx (+)] were kept at the Animal Center for Biomedical Research (University of Tokyo, Tokyo, Japan), according to the institutional guidelines. NOD/Shi-scid, IL-2γ null (NOG) mice were purchased from the Central Institute for Experimental Animals (Kawasaki, Japan).

Retrovirus production, BM harvest, and serial replating assays

To produce oncoprotein-expressing retrovirus, Plat-E packaging cells[23] were transiently transfected with retroviral constructs, as described previously.[24,25] To produce green fluorescent protein (GFP)– or Cre recombinase fused to the estrogen receptor (CreER)-GFP–expressing retrovirus, we used MP34 packaging cells transduced with pGCDNsam-enhanced (e)GFP (a gift from H. Nakauchi and M. Onodera, University of Tokyo) or pGCDNsam-eGFP-CreER. The viral supernatant was collected from the transfected Plat-E cells, filtered, and used for BM progenitor infection. Six- to 8-week-old female C57/B6 mice were primed with 3 mg of 5-fluorouracil 5 days before BM harvest (day 1). BM cells flushed from the tibia and femur were isolated by density centrifugation over Histopaque-1083 (Sigma-Aldrich) and were allowed to rest overnight in RPMI-1640 with 10% FCS, 1% penicillin streptomycin (PS), and cytokines (50 ng/mL SCF, 50 ng/mL megakaryocyte growth and development factor, 50 ng/mL fusion protein of IL-6R and IL-6, and 50 ng/mL Flt-3 ligand). The following day (day 2), the BM cells were combined with retroviral supernatant and RetroNectin (Takara). On day 4, the infected BM were harvested and resuspended in cold PBS (final concentration, $1 \times 10^4/\mu L$). Serial replating assays were performed at a density of 10^4/mL replated in duplicate every 7 days in Methocult 3434 (StemCell Technologies). BMS-345541 (Calbiochem) was reconstituted with DMSO (Sigma-Aldrich) and added to methylcellulose of the third generation colony-forming cells.

Microarray analysis

These procedures were performed as described previously.[25] Lineage-, Sca-1+, c-Kit+ (LSK) cells derived from AML1 f/f mice were transduced with GFP or CreER-GFP–expressing retroviruses. GFP-positive cells were sorted by an FACSAria cell sorter (BD Biosciences). Total RNA was prepared from sorted GFP+ cells after 24 or 48 hours from adding 4-hydroxytamoxifen (4-OHT; Sigma-Aldrich) using the RNeasy micro kit (QIAGEN). Amplification and biotin labeling of fragmented cDNA was carried out using the NuGen Ovation Biotin labeling system (NuGEN Technologies) in duplicate. Labeled probes were hybridized to the Mouse Genome 430 2.0 Array (Affymetrix) and scanned with a GeneChip Scanner 3000 7G (Affymetrix). Expression data were extracted from image files produced on GeneChip Operating software 1.0 (Affymetrix). Normalization and expression value calculation were performed using DNA-Chip Analyzer (www.dchip.org).[26] Normalized data were filtered for minimal expression and then tested for gene set enrichment using gene set enrichment analysis (GSEA) Version 2.0 (www.broad.mit.edu/gsea/).[27] GSEA enrichment results were filtered for statistical significance using a nominal P value threshold of .05. We also used gene expression data of 285 individuals with AML (www.ncbi.nlm.nih.gov/geo; accession GSE1159 [NCBI GEO])[28] and expression data of AML1/ETO transduced human cord blood cells (www.ncbi.nlm.nih.gov/geo; accessions GSE8023, GSE7011 [NCBI GEO]).[29,30]

Nuclear translocation assay

The HEK293T cells were cultured on glass coverslips and transfected with Lipofectamine (Invitrogen) according to the manufacturer's instructions. Thirty-six hours later, conditioning medium was replaced with starvation medium containing 0.5% FCS medium. Twelve hours later, 100 ng/mL TNF-α (Sigma-Aldrich) was added to the cells for 5 to 20 minutes. The cells were washed 3 times with PBS and fixed in 3.7% formaldehyde in PBS for 20 minutes. After washing with PBS, the cell membrane was permeabilized by treatment with 0.2% Triton in PBS for 10 minutes, and the cell membrane was blocked by treatment with 1% BSA in PBS for 40 minutes. The cells were treated with mouse anti-FLAG monoclonal antibody (dilution, 1:200; Sigma-Aldrich) and rabbit anti-p65 monoclonal antibody (dilution, 1:100; Santa Cruz Biotechnology) for 3 hours. After washing with PBS, the cells were stained with Alexa Fluor 555 goat anti-mouse IgG (dilution, 1:500; Invitrogen), Alexa Fluor 488 goat anti-rabbit IgG (dilution, 1:500; Invitrogen), and TO-PRO3 (dilution, 1:1000; Invitrogen) for 1 hour. The cells were washed and treated with ProLong Gold antifade reagent (Invitrogen), and the proteins were visualized using a confocal microscope (63×/1.4 NA oil objective, TCS-LS, Leica). FLAG-tagged AML1 mutants were inserted into pME18S expression vector.[24]

Quantification of nuclear p65

Nuclear intensity of p65 was quantified with ImageJ Version 1.41o software (National Institutes of Health).[31] Mean nuclear intensities of 10 cells from 2 pictures were quantified. Intensities were normalized by background subtraction.

Quantitative real-time PCR

Real-time PCR was performed using the ABI PRISM 7000 Sequence Detection System (Applied Biosystems) or LightCycler 480 (Roche Diagnostics) according to the manufacturers' instructions. Results were normalized to GAPDH levels. PCR primers used for quantitative PCR were as follows: Nfkb2f, ACCAAGCTCCATGCTAATGTGAAT; Nfkb2r, GGGTGTGTTTCCAGCAAAGGT; GAPDHf, TGGTGAAGCAGGCATCTGAG; GAPDHr, TGCTGTTGAAGTCGCAGGAG; Cd74f, GCAGTGGCTCTTGTTTGAGA; Cd74r, TTCCTGGCACTTGGTCAGTA; Nfkbiaf, CGAGGAGTACGAGCAAATGG; Nfkbiar, TGATTGCCAAGTGCAGGA; Nfkbief, CGACTCTCTGCTGCTGAATG; Nfkbier, GGTCATCGAAGGGCAAATAA; Plekf, CCGGCCTACCTGCACTACTA; Plekr, CAGCCTCTCAAGTGAACTGC; Tnfaip3f, AAGCTCGTGGCTCTGAAAAC; Tnfaip3r, CCCCACATGTACTGACAAGC; Birc3f, AGAGAGGAGCAGATGGAGCA; Birc3r, TTTGTTCTTCCGGATTAGTGC; Il2rgf, AGGCGAGCTGTACAGAAGCTA; Il2rgr, CTGGGATTCACTCAGATTGCT; Relbf, GCCTTGGGTTCCAGTGAC; and Relbr, TGTATTCGTCGATGATTTCCAA.

Flow cytometric analysis

Cells were sorted with an FACSAria cell sorter, and analysis was performed on an FACS LSRII flow cytometer (BD Biosciences). Intracellular staining of phospho-p65 was done according to the manufacturer's protocol (Cell

Signaling Technology). To gate AML1-transduced cells, we used Pcdef3-IRES-GFP or Pcdef3-IRES-GFP-AML1 vector.

Immunoprecipitation and Western blotting

For immunoprecipitation, cell lysates were incubated with the anti-FLAG M2 monoclonal antibody (Sigma-Aldrich), anti-AML1 monoclonal antibody (Cell Signaling Technology), normal rabbit IgG (Santa Cruz Biotechnology) for 1 hour at 4°C. Then, the samples were incubated with protein G-Sepharose (GE Healthcare) for 1 hour at 4°C. The precipitates were washed twice with the TNE buffer[32], twice with high salt–containing wash buffer (50mM Tris-HCl, pH 7.5, 500mM NaCl, 0.1% Nonidet P-40, and 0.05% sodium deoxycholate), and once with low salt–containing buffer (50mM Tris-HCl, pH 7.5, 0.1% Nonidet P-40, and 0.05% sodium deoxycholate), and they were subjected to sodium dodecylsulfate-polyacrylamide gel electrophoresis (SDS-PAGE) and analysis by Western blotting. Antibodies used in immunoblotting were as follows: anti-FLAG (Sigma-Aldrich), anti-hemagglutinin (HA; Roche Diagnostics), anti-AML1 (Cell Signaling Technology), anti-IKKα (Cell Signaling Technology), anti-IKKβ (Cell Signaling Technology), anti-IκBα (Cell Signaling Technology), anti-p65 (Cell Signaling Technology), anti–NF-κB2 p100/p52 (Cell Signaling Technology), and anti–β-actin (Cell Signaling Technology). ECL detection (GE Healthcare) was carried out according to the manufacturer's recommendations. Protein levels were quantified with ImageJ Version 1.41o software.[31] Nuclear fraction or cytoplasmic fraction was prepared using a nuclear extract kit (Active Motif) according to the manufacturer's instructions. Splenic B cells were separated by an auto-MACS separation column (Miltenyi Biotec) according to the manufacturer's protocol. These B cells were stimulated with 200 ng/mL recombinant human BAFF (BioSource) for 8 hours. HA-tagged AML1 mutants were inserted into pME18S expression vector.[24] FLAG-tagged IKKα and IKKβ were gifts from Dr T. D. Gilmore (Boston University, Boston, MA).

Leukemogenesis assays in vivo

These procedures were performed as described previously.[13] In brief, BM mononuclear cells were prestimulated and infected for 60 hours with the retroviruses harboring AML1 S291fsX300-IRES-GFP. Then, 0.2 to 1.2×10^6 infected BM cells (Ly5.1) were injected through the tail vein into C57/B6 (Ly5.2) recipient mice (8 weeks of age) that had been administered a sublethal dose of 5.25 Gy of total body γ-irradiation. In survival assays, 2×10^6 S291fsX300-induced leukemic spleen cells or 1×10^5 MLL/ENL-induced leukemic spleen cells were injected into sublethally irradiated (7.5 Gy) C57/B6 (Ly5.2) mice. Bortezomib (LC Laboratories) was administrated at doses of 1.0 mg/kg, given by intraperitoneal bolus injection twice weekly.

Orthotopic cell line model and in vivo bioluminescence imaging

These procedures were performed as described previously.[33] In brief, 1 million SKNO-1 cells were injected into sublethally irradiated (2.0 Gy) NOG mice via tail vein. One week after injection, bortezomib was administrated at doses of 1.0 mg/kg, given by intraperitoneal bolus injection twice weekly. Total body bioluminescence was determined by in vivo bioluminescence imaging (IVIS Lumina2; Caliper Life Sciences) and quantitated using Living Image 2.60 software (Caliper Life Sciences). Luciferase positive SKNO-1 cells were kindly provided by Dr Andrew L. Kung (Dana-Farber Cancer Institute, Boston, MA).

In vitro kinase assay

These procedures were performed as described previously.[34] In brief, HEK293T cells transiently expressing either AML1 or mock vector were treated with 100 ng/mL TNF-α (Sigma-Aldrich) for the indicated times and then harvested. Cell extracts were precipitated with anti-IKK antibody (Cell Signaling Technology) for 1 hour at 4°C, and protein G-Sepharose was added for 1 hour at 4°C. Immune complexes were washed twice with lysis buffer and then washed twice with kinase buffer (20mM HEPES, pH 7.4, 1mM $MnCl_2$, 5mM $MgCl_2$, 10mM β-glycerol phosphate, 0.1mM sodium orthovanadate, 2mM NaF, and 1mM dithiothreitol). Kinase assays were performed for 30 minutes at 30°C in 20 μL of kinase buffer containing 5 μCi of [γ-^{32}P]ATP (GE healthcare) and 1 μg of GST-IκBα (Millipore) as a substrate. The reaction mixtures were resolved by SDS-PAGE and then detected by autoradiography and quantified with ImageJ Version 1.41o software.[31]

Statistical analysis

To compare data between groups, unpaired Student *t* test was used when equal variance were met by F-test. When unequal variances were detected, the Welch *t* test was used. Differences were considered statistically significant at a *P* value of less than .05. To analyze the survival curve, log-rank (Mantel-Cox) test was used. These analysis were done using Prism 5 (GraphPad Software).

Results

NF-κB signaling is activated in AML1-deficient cells

To seek the therapeutic target in AML1-related leukemia, we investigated the deregulated signaling pathway induced by loss of AML1. We analyzed the change of gene expression profiles in immature hematopoietic cells induced by AML1 inactivation. We purified LSK cells as hematopoietic stem and progenitor cells from AML1 conditional knockout (cKO) mice and retrovirally transduced CreER into them.[35] Immediately after deleting AML1 by the activation of CreER with 4-OHT, we collected them and analyzed their gene expression profiles with oligonucleotide microarray (Figure 1A, and supplemental Figure 1A, available on the *Blood* Web site; see the Supplemental Materials link at the top of the online article). As a control, we used LSK cells infected with an empty retrovirus and treated them with 4-OHT. We confirmed that AML1 was efficiently deleted after the addition of 4-OHT (Figure 1B). To analyze their gene expression profiles, we used GSEA with molecular signature database.[27,36] First, we analyzed the expression profiles with all curated gene sets (C2) and found that sets of NF-κB–related genes are significantly enriched in AML1-deficient cells (AML1 flox/flox, CreER+, 24 and 48 hours after adding 4-OHT; Figure 1C-E and supplemental Figure 1B-D).[37-39] Next, we analyzed them with all motif gene sets (C3), and again we found that NF-κB–regulated genes are significantly enriched in the AML1-deficient cells (Figure 1F-H and supplemental Figure 1E-G). In addition, the target genes of NF-κB signaling detected in hematopoietic malignant cells were distinctly enriched in AML1-deficient cells (Figure 1I and supplemental Figure 1H).[21] We confirmed the elevated expression of NF-κB target genes by real-time PCR (Figure 1J). Because we added 4-OHT both to mock- and CreER-transduced cells, the effects of 4-OHT to our gene expression analysis are unlikely.

To confirm that NF-κB signaling is activated in AML1-deficient cells, we performed immunofluorescent staining of p65, a major component of NF-κB in the canonical pathway, in AML1-deficient hematopoietic progenitor cells. As shown in Figure 2A, nuclear localized p65 was increased in AML1-deficient cells (AML1 flox/flox, CreER). This increase was attenuated by BMS-345541, an inhibitor of IKK. We also found that nuclear p65 protein was increased in AML1-defficient hematopoietic progenitor cells by Western blotting (Figure 2B). In addition, transcription level of NFKB2, a major component of noncanonical NF-κB pathway, was increased in AML1-deficient cells (Figure 2C), compatible with the transcription of NFKB2 being regulated by p65.[18] In the noncanonical NF-κB pathway, cytokines such as BAFF promote processing

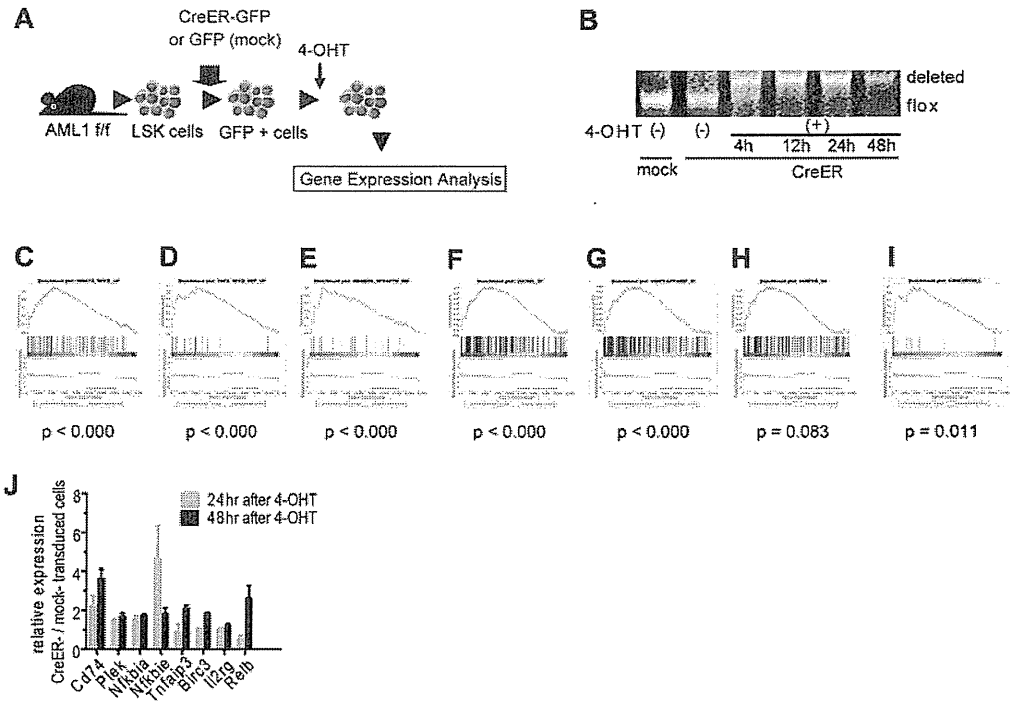

Figure 1. NF-κB signaling is activated in AML1-deficient cells. (A) Schematic representation of the gene expression analysis. LSK cells from AML1 cKO mice (AML1 f/f) were transduced CreER-GFP or GFP expressing retroviruses. GFP+ cells were sorted and were subjected to gene expression analysis 24 or 48 hours after adding 4-OHT. (B) PCR genotyping of BM cells from AML1 cKO mice after adding 4-OHT. (C-I) NF-κB–related gene sets enriched in AML1-defecient cells (AML1 flox/flox, CreER+ 24 and 48 hours after adding 4-OHT) by GSEA Version 2.0. (C) A gene set that includes genes up-regulated by NF-κB (HINATA_NFKB_UP). (D) A gene set that includes genes which are up-regulated TNF-α treatment (TNFA_NFKB_DEP_UP). (E) A gene set that includes Ras-inducible, NF-κB–regulated genes (HANSON_NFKAPPB_IND). (F) A gene set that includes genes with promoter regions containing REL motif (V$CREL_01); (G) a gene set which includes Genes with promoter regions containing p65 motif (V$NFKAPPAB65_01). (H) A gene set that includes genes with promoter regions containing NF-κB motif ($NFKB_Q6). (I) Target genes of NF-κB.[21] Nominal *P* value was estimated by GSEA software. (J) mRNA expression for NF-κB target genes in LSK cells transduced with CreER or mock from AML1 f/f mice 24 or 48 hours after 4-OHT addition. Error bars show mean ± SEM.

of p52 from p100 (NFKB2), protein level of which reflects activating status of the pathway. As shown in Figure 2D, both of basal and BAFF-mediated processing of p52 are augmented in AML1-deficient splenic B cells (AML1 flox/flox Mx+) compared with control cells (AML1 flox/flox Mx−) that express intact AML1. These data indicate that both canonical and noncanonical pathways of NF-κB signaling are aberrantly activated in AML1-deficient murine hematopoietic cells.

AML1 attenuates NF-κB signaling through interaction with IKK complex

Because the NF-κB signaling is activated by the loss of AML1, we investigated whether AML1 represses NF-κB signaling. We performed nuclear translocation assays using HEK293T cells. When HEK293T cells are starved with culture medium containing 0.5% FCS, p65 stays in the cytoplasmic fraction (Figure 3A top left panel). Twenty minutes after adding TNF-α, p65 translocates to the nuclear fraction (Figure 3A top right panel). In AML1-transduced cells, p65 does not translocate to nuclear fraction after adding TNF-α (Figure 3A bottom right panel). These data show that AML1 inhibits nuclear translocation of p65 when expressed in HEK293T cells (Figure 3A). TNF-α–induced phosphorylation of p65 at serine 536, which is important for its activation, also was inhibited by AML1 in those cells (Figure 3B).

To seek the underlying mechanism for inhibition of NF-κB signaling by AML1, we assessed physical and functional interaction between AML1 and signaling components of NF-κB signaling. IKK is a multimeric complex consisting of IKKα, IKKβ, and IKKγ. The kinase activity of IKK is essential for IκB degradation and nuclear translocation of p65 and is exerted by IKKα and IKKβ. As shown in Figure 4A-B, AML1 was coprecipitated with IKKα and IKKβ when they are expressed in HEK293T cells. These results indicate that AML1 physically interacts with IKKα and IKKβ. Using Jurkat cells, we confirmed that endogenous AML1 forms a complex with IKKα and IKKβ (Figure 4C). Because AML1 is a DNA-binding protein and IKK complex is thought to act mainly in the cytoplasm, we examined where they interact with each other. As shown in Figure 4D, interaction between AML1 and IKK complex was mainly detected in the cytoplasmic fraction in HEK293T cells. Interestingly, protein level of AML1 was increased in the cytoplasmic fraction when IKKα was overexpressed with AML1. We confirmed that endogenous AML1 physically interacts with IKK complex mainly in the cytoplasmic fraction in Jurkat cells (Figure 4E). We also confirmed that AML1 physically interacts with IKK complex in U937 cells, a human myeloid cell line (Figure 4F). Next, we tested whether AML1 affects the kinase activity of IKK complex. Using the in vitro kinase assay, we found that AML1 significantly suppresses the kinase activity of IKKα and IKKβ (Figure 4G-H). In accordance with these findings, AML1 significantly attenuated TNF-α–induced degradation of IκBα in HEK293T cells (Figure 4I).

Taken together, AML1 acts as a cytoplasmic attenuator of IKK complex, thus accounting for a mechanistic basis for the inhibition of NF-κB signaling by AML1. Suppression of IKK activity by

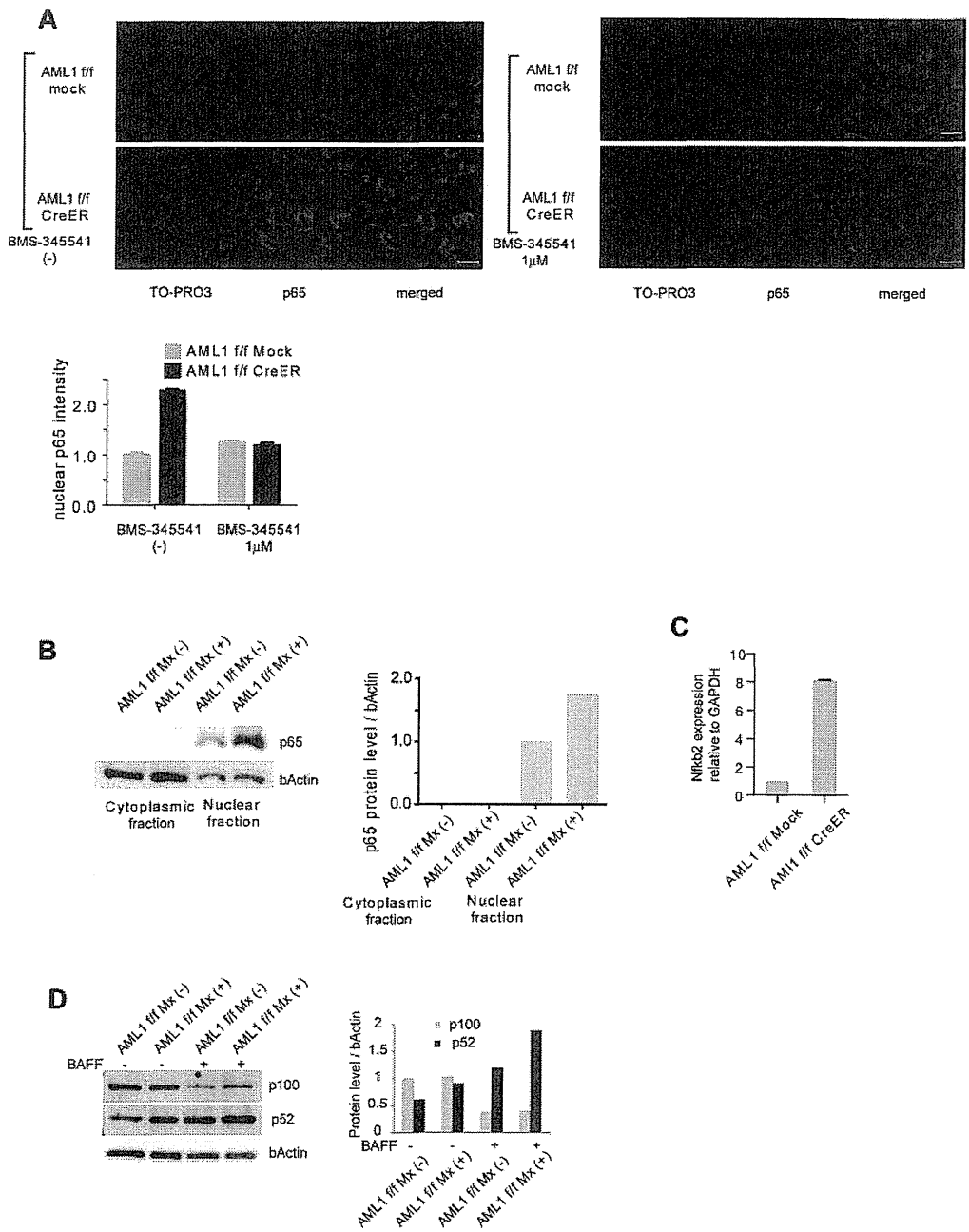

Figure 2. Canonical and noncanonical pathways of NF-κB signaling are activated in AML1-deficient cells. (A) Immunofluorescent staining of p65 in c-kit + BM cells transduced with CreER or mock from AML1 flox/flox (f/f) mice with or without BMS-345541 (1 μM). Scale bar represents 10 μm. Blue indicates TO-PRO3 (nucleus), and red indicates p65. The mean intensity of nuclear localized p65 was quantified with ImageJ Version 1.41o software.[31] (B) Fractionated Western blotting of p65 in c-kit + BM cells of AML1-deficient (AML1 f/f Mx+), or control (AML1 f/f Mx−) mice. (C) NFKB2 mRNA expression in BM cells transduced with CreER or mock from AML1 f/f mice 48 hours after 4-OHT addition. Error bars show mean ± SEM (D) Western blotting of NFKB2 (p100 or p52) in B220 + spleen cells from AML1 cKO mice (AML1 f/f Mx+) or control mice (AML1 f/f Mx−) with or without BAFF (200 ng/mL). Protein levels were quantified with ImageJ Version 1.41o software.[31]

AML1 results in the inhibition of both nuclear translocation of p65 and activation of NF-κB target genes.

Critical role for NF-κB signaling in the myeloid transformation induced by AML1 mutants

Next, we analyzed the contribution of NF-κB signaling to AML1-related myeloid transformation. We found that 3 types of AML1 mutants, A224fsX228, S291fsX300, and R293X, can transform bone marrow cells in a serial replating assay (Figure 5A and supplemental Figure 2A). A224fsX228 and S291fsX300 were found in human cases with MDS. Similar types of mutants, N209fsX233, R290fsX299, and V292fsX300, were found in cases with de novo AML. R293X was found in both cases with MDS and de novo AML. These mutants belong to the C-terminally truncated type.[3,5,40] Among these mutants, it was recently reported that S291fsX300 induce AML in a mouse BMT model, indicating the in vivo transforming activity of this mutant.[13] We first assessed the effect of S291fsX300 overexpression on NF-κB signaling. Remarkably, in contrast to the wild type of AML1, S291fsX300 did not inhibit p65 nuclear

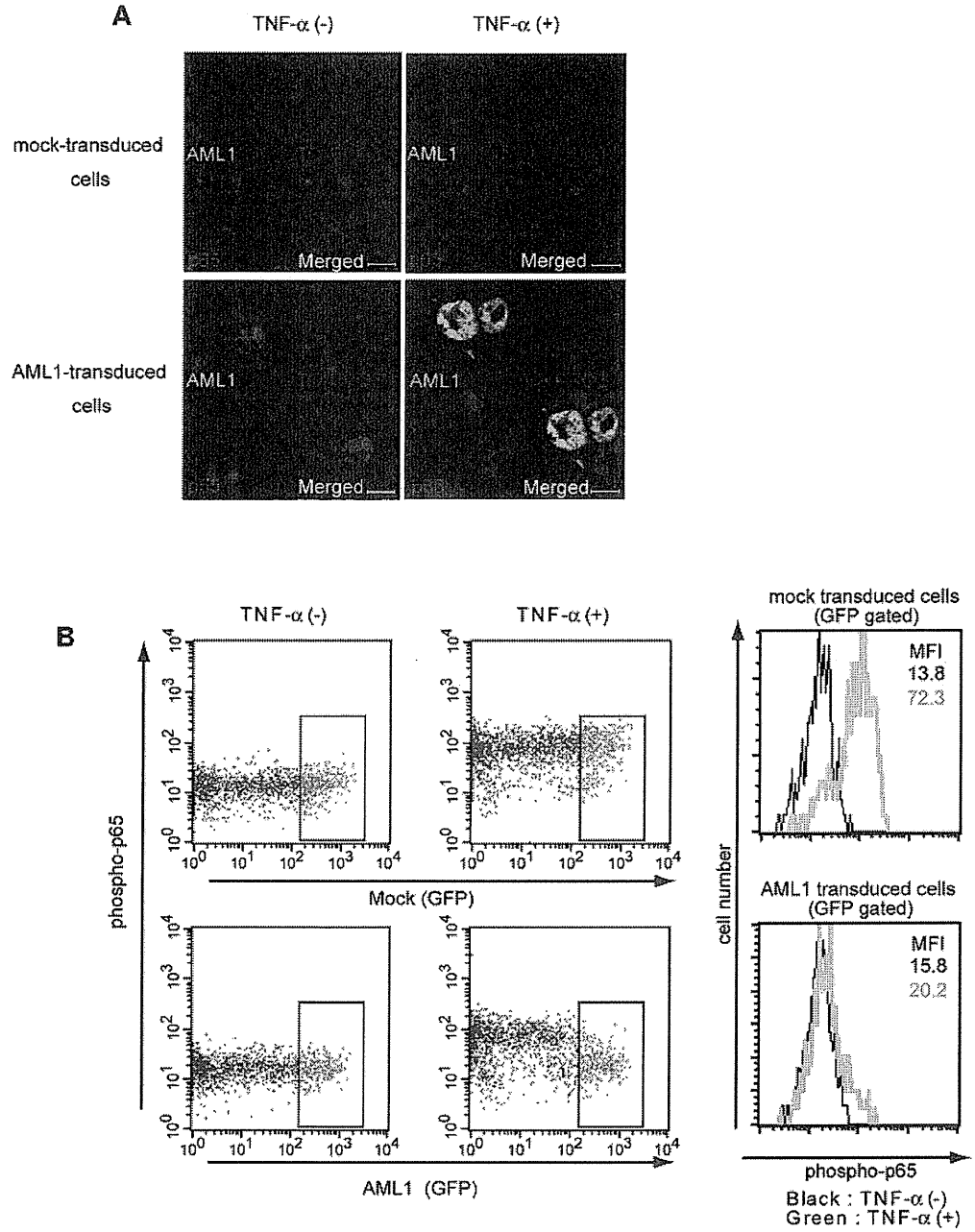

Figure 3. AML1 inhibits nuclear translocation and phosphorylation of p65. (A) Nuclear translocation assays of p65 in HEK293T cells transduced with AML1 or mock, 20 minutes after the addition of TNF-α. Scale bar represents 10 μm. Green indicates AML1; blue indicates TO-PRO3 (nucleus); and red indicates p65. (B) Intracellular FACS analysis of phospho-p65 (Ser 536) in HEK293T cells transduced with AML1 or mock. GFP-positive fractions were gated. Green line shows phosphorylated p65 protein 5 minutes after TNF-α stimulation. MFI indicates mean fluorescence intensity.

translocation induced by TNF-α (Figure 5B-C). As is compatible with these findings, S291fsX300 has lost the ability to repress kinase activities of IKKα and IKKβ (Figure 5D-E). In addition, neither A224fsX228 nor R293X inhibited p65 nuclear translocation (Figure 5F-G). In accordance with the inability to inhibit NF-κB signaling, replating capacity of the bone marrow cells introduced with these 3 mutants was highly susceptible to the pharmacologic inhibition of NF-κB signaling by BMS-345541 (Figure 5H). In-frame mutation in the Runt domain such as D171N is another type of AML1 abnormality frequently found in MDS patients (supplemental Figure 2B).[12] We found that D171N also did not inhibit p65 nuclear translocation (supplemental Figure 2C). Consistently, the inhibitory effect against IKK activity of D171N was attenuated (supplemental Figure 2D-E). These results suggest that the loss of inhibition of NF-κB signaling is a critical mechanism shared by many types of AML1 mutants in the development of AML.

To seek the NF-κB inhibitory domain of AML1, we analyzed a series of deletion mutants of AML1 in nuclear translocation assays of p65 (supplemental Figure 3A). As shown in supplemental Figure 3B, AML1 Δ444, which lacks the domain interacting with a corepressor TLE, inhibited p65 nuclear translocation, whereas AML1 Δ335, AML1a, a truncated isoform of AML1, or AML1 ΔRunt did not (supplemental Figure 3B). These data

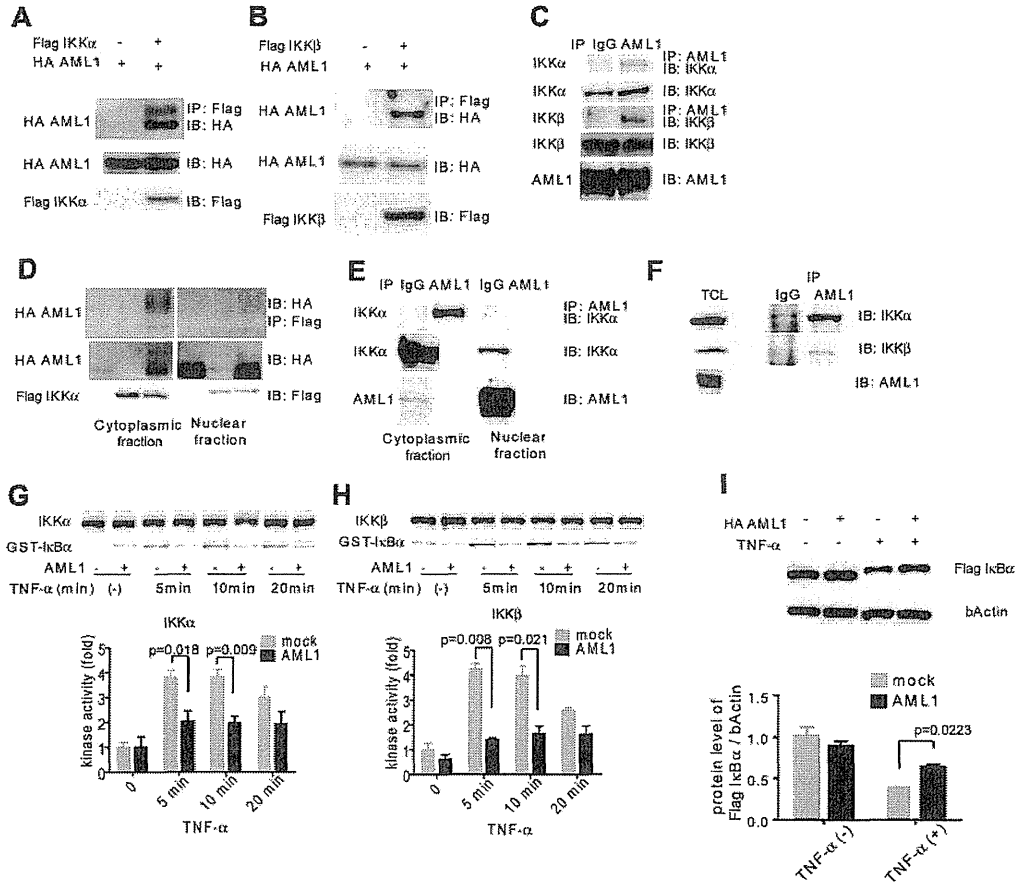

Figure 4. AML1 physically interacts with IKK complex and inhibits its kinase activity. (A-B) Interaction between AML1 and IKK complex. HEK293T cells were transfected with plasmids encoding for HA-AML1, FLAG-IKKα (A) and FLAG-IKKβ (B), as indicated, and extracts were immunoprecipitated with the antibody against FLAG. Western blots of the input lysate or immunoprecipitates were analyzed using the indicated antibodies. (C) Endogenous interaction between AML1 and the IKK complex in Jurkat cells. Cell extract from the Jurkat cells was immunoprecipitated with the antibody against AML1. Western blots of the input lysate or immunoprecipitates were analyzed using the indicated antibodies. (D) Interaction between AML1 and the IKK complex in cytoplasmic or nuclear fraction in HEK293T cells. (E) Endogenous interaction between AML1 and the IKK complex in cytoplasmic or nuclear fraction in Jurkat cells. (F) Endogenous interaction between AML1 and the IKK complex in U937 cells. Cell extract from the U937 cells was immunoprecipitated with the antibody against AML1. Western blots of the total lysate or immunoprecipitates were analyzed using the indicated antibodies. (G-H) In vitro kinase assays of IKKα (G) or IKKβ (H) in HEK293T cells transduced with AML1 or mock. Kinase activities were detected by autoradiography and quantified with ImageJ Version 1.41o software.[31] Error bars show mean ± SEM. (I) Western blotting of IκBα degradation in HEK293T cells transduced with AML1 or mock. Protein levels of IκBα were quantified with ImageJ Version 1.41o software.[31] Error bars show mean ± SEM.

indicate that C-terminal region with intact Runt domain of AML1 is required for inhibition of p65 nuclear translocation. We also assessed the physical interaction between each mutant of AML1 and IKK and found that all of the employed mutants retain the ability to interact with IKKα (supplemental Figure 3C). In addition, we found that D171N and S291fsX300 can interact with IKKα (supplemental Figure 2F). These results indicate that besides the physical interaction, there exists some additional mechanism that requires the integrity of AML1 for efficient inhibition of NF-κB by AML1.

AML1/ETO-positive leukemia is dependent on NF-κB signaling

Formation of chimeric genes because of chromosomal translocation is a major cause of AML1 dysfunction that leads to human leukemia. Among them, AML1/ETO, generated in t(8;21) leukemia, is one of the most frequent chimeric genes found in human leukemia. We examined how AML1/ETO affects NF-κB signaling. In contrast to AML1, AML1/ETO could not block nuclear translocation of p65 (Figure 6A). As is compatible with this observation, AML1/ETO has lost the ability to inhibit the kinase activity of IKKα and IKKβ, although it can physically interacted with IKKα (Figure 6B-C and supplemental 4A). In addition, mouse bone marrow cells transformed by AML1/ETO showed enhanced nuclear localization of p65 compared with those immortalized by MLL/ENL (Figure 6D). In agreement with these findings, the growth of AML1/ETO-transformed cells was more susceptible to the NF-κB inhibitor BMS-345541, compared with MLL/ENL-transformed cells (Figure 6E-F). These results indicate a critical role of NF-κB signaling in hematopoietic cell transformation by AML1/ETO.

To evaluate activation of NF-κB signaling by AML1/ETO in human hematopoietic cells, we first used Kasumi-1 cells, a cell line derived from AML1/ETO-positive leukemia, and we examined their susceptibility to NF-κB inhibition. In Kasumi-1 cells, small amounts of AML1 and AML1/ETO were detected in the cytoplasmic fraction (supplemental Figure 4B). As shown in Figure 6G, proliferation of Kasumi-1 cells was more sensitive to BMS-345541 than that of THP-1 cells, a human leukemia cell line expressing MLL/AF9. Next, we analyzed in silico the previously reported gene expression data of human leukemias by Valk et al.[28] As shown in supplemental Figure 4C, NF-κB signaling was strongly activated in cluster 5, which was defined

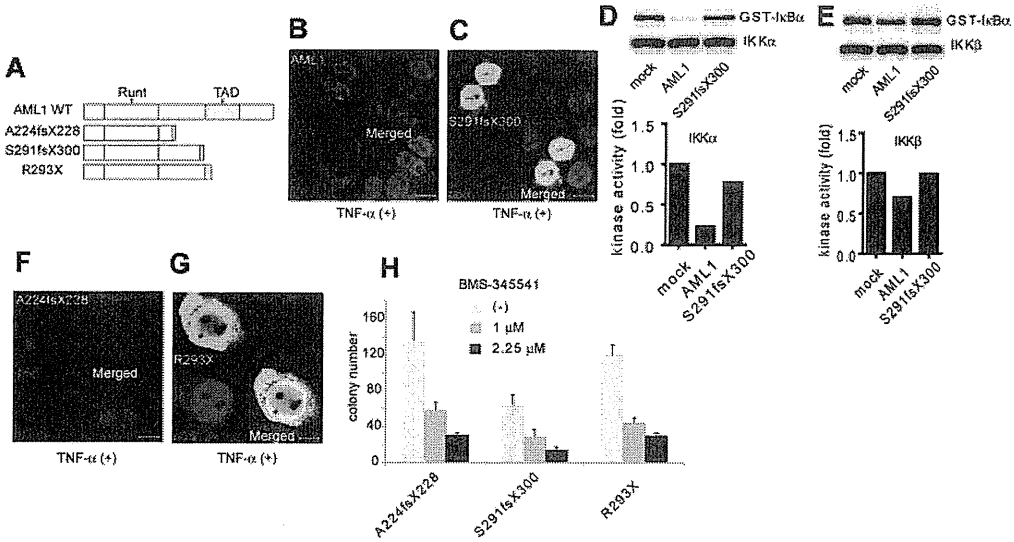

Figure 5. A critical role of NF-κB signaling in the myeloid transformation induced by AML1 mutants. (A) Schematic presentation of structures of the AML1 mutants. Runt indicates Runt domain, and TAD indicates transactivating domain. (B-C) Nuclear translocation assays of p65 in HEK293T cells transduced with AML1 mutants as indicated, 20 minutes after the addition of TNF-α. AML1 (B) and S291fsX300 (C). Scale bar represents 10 μm. (D-E) In vitro kinase assays of IKKα (D) or IKKβ (E) in HEK293T cells transduced with AML1 or S291fsX300, 20 minutes after the addition of TNF-α. Kinase activities were detected by autoradiography and quantified with ImageJ Version 1.41o software.[31] (F-G) Nuclear translocation assays of p65 in HEK293T cells transduced with AML1 mutants as indicated, 20 minutes after the addition of TNF-α. A224fsX228 (F) and R293X (G). Scale bar represents 10 μm. (H) Colony counts from the serial replating assays of AML1-mutants-transformed cells with BMS-345541. Error bars show mean ± SEM.

by Valk et al according to gene expression profiles.[28] Remarkably, NF-κB signaling was activated in cluster 13, which contains patients with t(8;21), compared with any other clusters except cluster 5 (Figure 6H and supplemental Figure 4D). These results again indicate that NF-κB signaling is activated in AML1/ETO-positive leukemia and suggest that deregulated NF-κB signaling plays a significant role in AML1/ETO-induced transformation of hematopoietic cells.

Bortezomib ameliorates AML1-related leukemia in vivo

To assess the consequence of NF-κB inhibition on AML1-related leukemia in vivo, we used a mouse BMT model of AML1 S291fsX300.[13] We isolated spleen cells from leukemic mice that express AML1 S291fsX300 and transplanted them into sublethally irradiated (7.5 Gy) C57/B6 mice. These mice were treated with twice weekly injections of vehicle or bortezomib, a proteasome inhibitor that broadly inhibits NF-κB signaling (Figure 7A). As shown in Figure 7B, bortezomib significantly prolonged survival of the recipient mice compared with the vehicle-treated mice. Given that NF-κB signaling is not activated in MLL leukemia (Figure 6D-G), we used another leukemia mouse model generated by MLL/ENL as a control that is independent of NF-κB signaling. In contrast to the case with AML1 S291fsX300, bortezomib could not prolong survival of MLL/ENL leukemia mice (Figure 7C).

Next, we examined whether bortezomib can suppress AML1/ETO-induced leukemia in vivo. Because retroviral transduction of AML1/ETO alone cannot induce leukemia in mice,[41] we used an orthotopic cell line model of luciferase-positive SKNO-1 cells, a human AML cell line that expresses AML1/ETO (Figure 7D).[33] We transplanted SKNO-1 cells into sublethally irradiated NOG mice via tail vein and treated these mice with vehicle or bortezomib. Tumor burden was quantified using in vivo bioluminescence imaging. Mice were intraperitoneally injected with 150 mg/kg luciferin and imaged them with an IVIS imaging system 10 minutes after injection. Total body bioluminescence was determined by in vivo bioluminescence imaging (IVIS Lumina2; Caliper Life Sciences) and quantitated using Living Image 2.60 software. In accordance with our results in vitro and in silico (Figure 6E-H), bortezomib significantly inhibited the growth of SKNO-1 cells in vivo (Figure 7E-F). Although bortezomib may have effects besides the NF-κB signaling inhibition, these results indicate that NF-κB signaling plays a critical role in the pathogenesis of myeloid tumors with deregulated AML1 function in vivo.

Discussion

In this study, we found that targeted disruption, as well as leukemia-related gene alteration, of *AML1* results in the aberrant activation of NF-κB signaling. To detect immediate targets of AML1, we analyzed the gene expression profiles of LSK cells just after the synchronous inactivation of AML1 using the CreER system, and we captured the immediate alteration of target gene expression that is sometimes hidden by cell population shift or secondary changes in cellular signaling. Although changes in the expression of individual target genes were relatively subtle, we successfully identified NF-κB signaling to be a target subject to immediate regulation of AML1. The in vitro synchronous inactivation system may provide us with a useful tool that can find unidentified target signaling of transcription factors. Furthermore, by determining expression of several genes related to NF-κB signaling, we can select patients who are candidates for NF-κB–targeted therapy. This strategy should be effective especially when genetic mutations are unknown. Previously, Valk et al made unsupervised cluster analyses and identified 16 clusters of patients with AML on the basis of gene expression profiles.[28] We reanalyzed their gene expression data in silico and found that NF-κB signaling is highly activated in a cluster previously identified as "cluster 5." Valk et al found that cluster 5 was associated with poorer prognoses but that specific genetic changes have not been identified in this

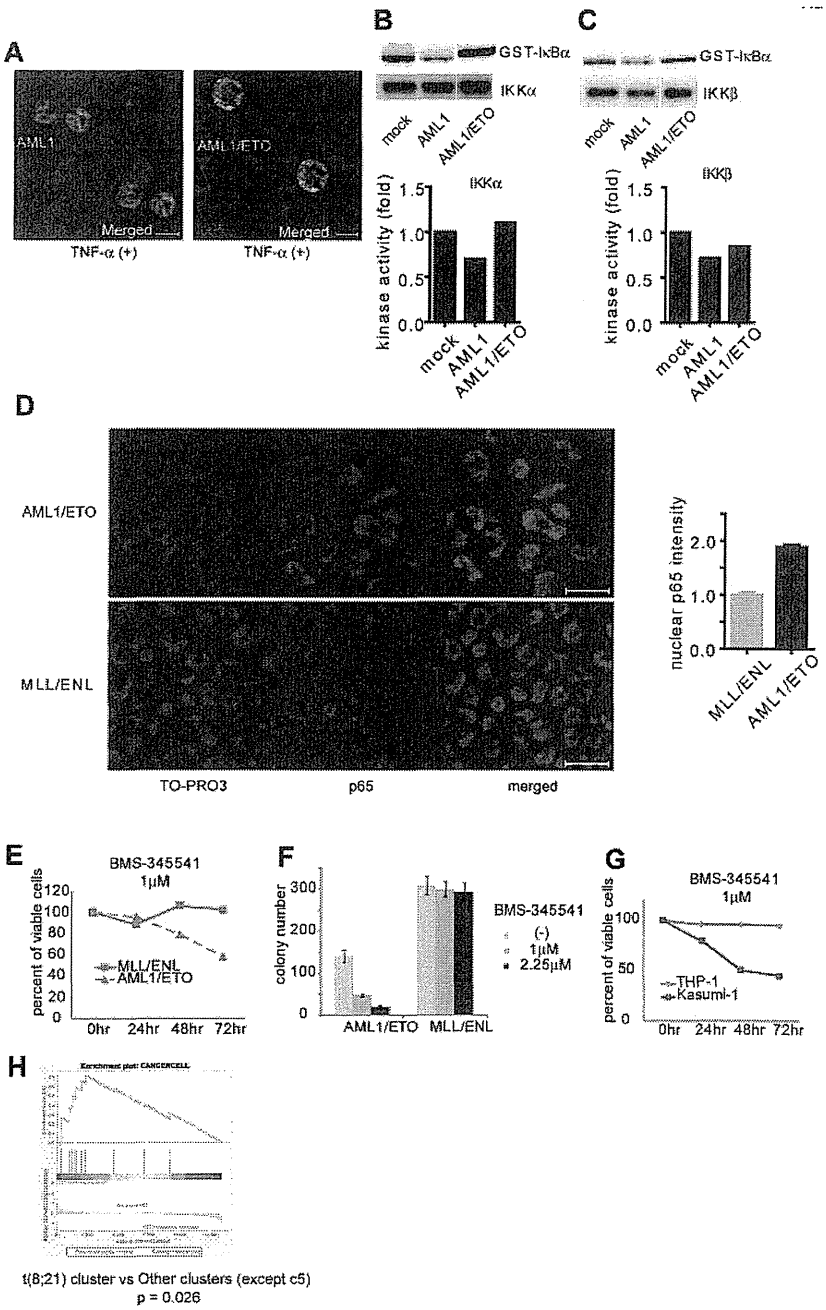

Figure 6. AML1/ETO-induced leukemic cells depend on NF-κB signaling. (A) Nuclear translocation assays of p65 in HEK293T cells transduced with AML1 (left) or AML1/ETO (right), 20 minutes after the addition of TNF-α. Scale bar represents 10 μm. (B-C) In vitro kinase assays of IKKα (B) or IKKβ (C) in HEK293T cells transduced with AML1 or AML1/ETO, 20 minutes after the addition of TNF-α. (D) Immunofluorescent staining of p65 in the BM cells transformed with AML1/ETO (top) or MLL/ENL (bottom). Scale bar represents 10 μm. Blue indicates TO-PRO3 (nucleus), and red indicates p65. The mean intensity of nuclear localized p65 was quantified with ImageJ Version 1.41o software.[31] (E) Comparison of sensitivities between AML1/ETO-transformed cells with MLL/ENL-transformed cells in liquid culture. (F) Colony counts from the serial replating assay of AML1/ETO- or MLL/ENL-transformed cells with BMS-345541. Error bars show mean ± SEM (G) Comparison of sensitivities between Kasumi-1 cells (AML1/ETO) with THP-1 cells (MLL/AF9) in liquid culture. (H) Enrichment of NF-κB target genes in t(8;21) leukemia cluster (c13) compared with other clusters (except c5).[28]

cluster.[28] In addition to t(8;21)–positive leukemia, the clinical activity of NF-κB inhibitors in AML cases belonging to this cluster warrants further investigation.

Although *AML1* mutations that lead to functional impairment have been frequently discovered in AML and MDS, it remains very difficult to develop a molecularly targeted therapy against deregulated AML1 function, as is often the case with leukemia-related transcription factors. We discovered that NF-κB signaling is distinctly activated as a consequence of *AML1* mutation found in human leukemia. In the current study, bortezomib, a clinically available drug that can inhibit NF-κB signaling, has shown a significant activity against AML1-related leukemia. A wide variety of small molecules that inhibit NF-κB signaling are now being developed and can become attractive candidates for targeted therapy of AML1-related leukemia in the future.

Although the amount of AML1 in the cytoplasm is lower than that in the nucleus, we show that the physical interaction between AML1 and IKK complex mainly occurs in the cytoplasm. In addition, the finding that AML1 inhibits the nuclear translocation of p65 that is tightly regulated by the cytoplasmic IKK complex supports the cytoplasmic function of AML1. Although nuclear exporting signal was not reported in AML1, IKK may export AML1 to the cytoplasmic fraction. We identified both AML1 and AML1/ETO protein in the cytoplasmic fraction of Kasumi-1 cells in supplemental Figure 4B. The amounts of AML1 and AML1/ETO protein in the cytoplasm are

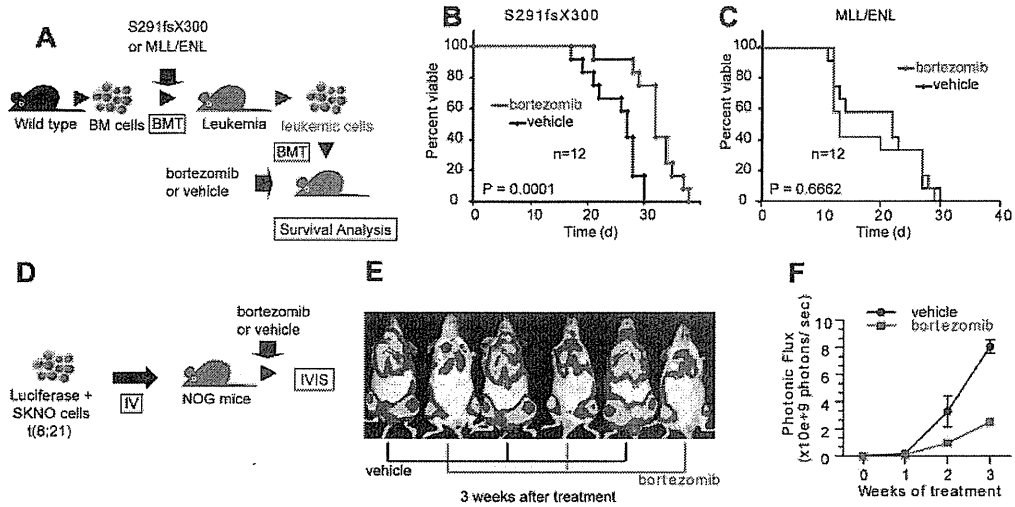

Figure 7. Bortezomib inhibits the proliferation of leukemic cells with AML1 S291fsX300 or AML1/ETO in vivo. (A) Schematic representation of the following experiments. Spleen cells isolated from S291fsX300-expressing leukemia mice were transplanted into sublethally irradiated (7.5 Gy) recipient mice. These mice were treated with twice weekly injections of vehicle or bortezomib. (B) Survival curves of mice transplanted with S291fsX300-induced leukemic cells treated with vehicle or bortezomib. Each group contains 12 mice. (C) Survival curves of mice transplanted with MLL/ENL-induced leukemic cells treated with vehicle or bortezomib. Each group contains 12 mice. The overall survival of mice in BM transplantation assays was analyzed by log-rank (Mantel-Cox) test. (D) Schematic representation of the following experiments. Luciferase positive SKNO-1 cells were injected into sublethally irradiated (2.0 Gy) NOG mice via tail vein, and these mice were treated with twice weekly injections of vehicle or bortezomib. (E-F) Tumor burden was quantified using in vivo bioluminescence imaging. Each group contains 3 mice.

fairly small. One possibility is that these proteins translocate between the cytoplasm and the nucleus in a context dependent manner. Another possibility is that AML1/ETO sequesters some components necessary for AML1 to inhibit IKK complex. A function of transcription factors that is exerted in the cytoplasm is well documented in p53.[42] Besides acting in the nucleus as a transcription factor to regulate expression of genes involved in apoptosis and cell cycle regulation, p53 triggers apoptosis and inhibits autophagy in the cytoplasm through a variety of processes, including induction of mitochondrial outer membrane permeabilization, direct regulation BAX activity, inhibition of AMP-dependent kinase, and activation of mammalian target of rapamycin. Revealing cytoplasmic functions of transcription factors will provide a new perspective for the therapy against malignancy with deregulated transcription factors.

Our data, however, do not deny the contribution of the transcriptional function of AML1 in inhibiting NF-κB signaling. It may be possible that AML1 attenuates NF-κB signaling transcriptionally and via the inducible IKK complex like Notch1.[20]

AML1 mutants including AML1/ETO tested in our study fail to inhibit kinase activity of IKKs, although they can physically interact with IKK complex. Therefore, it is likely that additional mechanism exists for wild-type AML1 to repress IKK activity after binding to IKK complex, which should be inactivated in AML1 mutants. One possible mechanism is that AML1 disturbs the formation of IKK complex. Another possibility is that AML1 blocks the interaction between IKK complex with upstream kinase or downstream substrates, such as IκBα or p65. Importantly, critical for the repression of IKK is C-terminal region, a region that may directly inhibit the IKK complex or to which some cofactor may bind. D171N cannot repress IKK activity, although it possesses the intact C-terminal region, and a conformational change caused by the point mutation may impair the inhibitory effect against IKK. Because AML1 mutants in this study can bind to IKK complex but do not attenuate IKK activity, it is assumed that they exert a dominant-negative effect against wild-type AML1.

In normal hematopoiesis, AML1 suppresses NF-κB signaling and thus may contribute to inhibition of excessive proliferation of hematopoietic cells. Aberrant activation of NF-κB signaling may cause expansion of HSCs in AML1 cKO mice. Although it is reported that neither p65 nor a constitutively active form of IKK increases the number of human cord blood cells when transduced in vitro, intact AML1 may inhibit the NF-κB signaling in these cells.[43] It also is reported that NF-κB signaling is more activated in leukemic stem cells than normal HSCs.[44] In leukemic cells, the NF-κB inhibitory mechanism including AML1 may be disrupted. Once genetic mutation of *AML1* occurs in hematopoietic cells, aberrant activation of NF-κB signaling exerts antiapoptotic and proliferation-promoting effects via activation of BCL-XL or JUNB. Proliferative advantage conferred by activated NF-κB signaling may contribute to the clonal evolution of AML1-mutated cells that leads to leukemic transformation. Conversely, it is known that activation of NF-κB signaling causes myeloproliferative disease via the stroma-mediated signaling.[45] Thus, germ line mutation of *AML1* that occurs in familial platelet disorder patients may contribute to leukemogenesis in those patients not only via a hematopoietic cell-autonomous function but also via niche-derived signaling.[7]

Both of AML1 and NF-κB play important roles in lymphocyte differentiation.[11,46] Well documented is the pathogenetic significance of NF-κB signaling in autoimmune diseases, especially rheumatoid arthritis (RA).[47] Disease-associated single-nucleotide polymorphisms in autoimmune diseases are found in AML1 binding sites of several gene promoters: SLC9A3R1 and NAT9 in psoriasis; SLC22A4 in RA; and PDCD1 in systemic lupus erythematosus.[48-50] A single-nucleotide polymorphism in AML1 per se also is associated with RA.[49] Along with this study, AML1 may contribute to the pathogenesis of autoimmune diseases through the cytoplasmic function to modulate NF-κB activity as well as the nuclear function as a transcription factor.